Comparison of spin dynamics in $YBa_2Cu_3O_{7-\delta}$ and $La_{2-x}Sr_xCuO_4$: Effects of Fermi-surface geometry

Qimiao Si,* Yuyao Zha, and K. Levin
Department of Physics and the James Franck Institute and Science and Technology Center for Superconductivity, The University of Chicago, Chicago, Illinois 60637

J. P. Lu
Physics Department, University of Illinois/Urbana-Champaign, 1110 W. Green Street, Urbana, Illinois 61801
(Received 15 October 1991)

Neutron experiments have indicated that the structure factor $S(\mathbf{q},\omega)$ for the two cuprates $YBa_2Cu_3O_{7-\delta}$ and $La_{2-x}Sr_xCuO_4$ has a different $\mathbf{q}$ dependence. Commensurate peaks at $(\pi/a,\pi/a)$ are observed in the former case, whereas clearly incommensurate peaks are seen in the latter, for metallic hole concentrations. We attribute this contrasting $\mathbf{q}$ dependence to differences in the Fermi-surface geometry, obtained in band-structure approaches, and (for the YBaCuO system) also corroborated by photoemission experiments. Using a large Coulomb-U, Fermi-liquid-based scheme, we present results for the $\mathbf{q},\omega$ and temperature dependence of the neutron cross section as well as for the temperature dependence of the NMR relaxation, in both cuprate families at various hole concentrations. When antiferromagnetic quasiparticle interactions of moderate strength are included, these calculations compare favorably with experiment. It should be stressed that the Fermi-surface shape must be accurately represented in both systems in order to produce this good agreement with the neutron data. We conclude that the close correspondence found, thus far, between band-structure-derived spin dynamics and the detailed fermiology of both cuprates provides support for Fermi-liquid-based schemes. Furthermore, this correspondence suggests important constraints which should be included in theoretical schemes ranging from the marginal and nearly antiferromagnetic Fermi liquid to more exotic scenarios for the normal state. Within this context, it is extremely important to determine the characteristic energy scales of the Fermi liquid. Comparison of our calculations with the measured energy scales of the spin dynamics indicates that these are sufficiently low so that one can reconcile deviations from canonical behavior above T_c with a Fermi-liquid ground state. Explicit effects of these low-energy scales are discussed in the context of the quasiparticle lifetime as a function of frequency and temperature. Our detailed studies also yield predictions for future experiments which will help to test futher the validity of this approach.

I. INTRODUCTION

It is widely believed that the spin dynamical properties of the cuprates contain valuable information about the normal state and possibly also the superconducting mechanism. The behavior of the dynamical structure factor $S(\mathbf{q},\omega)$ has been elucidated through both NMR (Ref. 1) and neutron measurements.[2-5] What is intriguing about these data, however, is the variation from one cuprate to another. Incommensurate peaks (which become increasingly more incommensurate with hole concentration x) are observed in the La-Sr-Cu-O family,[2,5] whereas commensurate structure at the $(\pi/a,\pi/a)$ point is found in Y-Ba-Cu-O systems.[3,4] In this paper we show that these differences are necessary consequences of Fermi-liquid-based theories of the cuprates and reflect important differences in the calculated band structure.

The magnetic properties of these Fermi-liquid-like schemes depend on the dynamical susceptibility of the noninteracting system (Lindhard function) $\chi^0(\mathbf{q},\omega)$, which in turn is based on the energy band dispersion. (Further corrections to the Lindhard function contribution may occur through residual quasiparticle interactions $J_H(\mathbf{q})$, deriving, for example, from superexchange and Ruderman-Kittel-Kasuya-Yosida (RKKY) effects.) In this way, the spin dynamics is intimately connected with the band structure. That one may view neutron measurements as a form of Fermi-surface spectroscopy is an important theme of the present paper.

It is now apparent that the Fermi surfaces of the cuprates are not universal in shape. Photoemission experiments[6] on Y-Ba-Cu-O corroborate the results of band-structure calculations[7] for the Fermi surface in the fully oxygenated system. Recent data at reduced oxygen stoichiometries also appear consistent with this shape.[8] This Fermi surface is rotated by 45° with respect to the predictions of the simple nearest-neighbor tight-binding band-structure scheme. It has been speculated that this rotation results from the interaction of the apical oxygen with the planar Cu.[9] While there are no angle-resolved photoemission data on La-Sr-Cu-O, it is reasonable to assume that in this system the Fermi-surface shape is also adequately described by the local-density-approximation (LDA) scheme,[10] so that it corresponds to the simple tight-binding "diamondlike" shape, slightly modified by higher-order hopping processes. Associated with these

differences in the band structure of Y-Ba-Cu-O and La-Sr-Cu-O are different nesting and Van Hove structures which enter into the Lindhard functions and thus into the neutron cross section.

Our approach, which is based on Fermi-liquid theory, shares many features with other Fermi-liquid scenarios in the literature. Our understanding of the rotated Fermi surfaces in Y-Ba-Cu-O builds on the LDA band-structure calculations of Pickett,[11] Anderson,[9] and Freeman[7] and their co-workers. Indeed Pickett was the first to note that the planar Fermi surfaces of the Y-Ba-Cu-O family seem inconsistent with the observed commensurate magnetic order of the parent magnetic insulator. This situation is in contrast to that in La-Sr-Cu-O where the nesting vector found in the metallic state is close to the wave vector for long-range magnetic order of the insulator. Newns, Pattnaik, and Tsuei[12] have explored a similar large-U, Fermi-liquid approach with particular recent emphasis on Van Hove effects and less attention on magnetic effects. Finally Ruvalds and Virosztek[13] have discussed extensively a variety of different experiments in the context of their nested Fermi-liquid theory. Although our Fermi surfaces appear to be less strongly nested than those they use, the present calculations also incorporate some of these near-nesting effects insofar as they are represented in the LDA calculated fermiology.

Thus far, the differences in the band structure in La-Sr-Cu-O and Y-Ba-Cu-O have not been included in theories which address neutron and NMR data. Nor has there been any substantial effort to explain the evidently contrasting behavior of the spin dynamics observed in neutron experiments. In this paper we explore the differences between these two cuprates using as a basis of our previous calculations[14,15] of the dynamical susceptibility $\chi(\mathbf{q},\omega)$ and including quasirealistic models of the band structure.[16] Within our random-phase-approximation- (RPA-) like theory, the dynamical susceptibility contains a competition between nesting effects [through the Lindhard function $\chi^0(\mathbf{q},\omega)$] and exchange effects which result from a (primarily) nearest-neighbor antiferromagnetic interaction, $J_H(\mathbf{q})$.[14] The different $\mathbf{q}$-space topography observed experimentally in $S(q,\omega)=\mathrm{Im}\chi(\mathbf{q},\omega)/(1-e^{-\omega/kT})$ for the two cuprates can be explained within this formalism, provided a quasirealistic Fermi-surface shape is assumed and the exchange interactions are of moderate strength.

We stress that this $\mathbf{q}$ structure is also associated with different temperature and frequency dependences in the two cuprates. The calculated (ω,T) behavior seems to compare favorably with measurements of the spin dynamics[1-5] and provides important insight into the *energy scales* of the Fermi liquid.[17] Indeed, studies of the various low energies are critical for determining the breakdown of canonical Fermi-liquid behavior with increasing temperature or frequency.[17] Further elucidation of this point is provided by our calculations of the quasiparticle lifetime as a function of ω (relevant to photoemission experiments) and temperature (relevant to resistivity data). In this context we note that the linear dependences on ω and T seen in photoemission and transport data are compatible with a Fermi-liquid ground state. The canonical Fermi-liquid ω^2 or T^2 dependences appear only at sufficiently low energies or temperatures; above the "crossover" energy scales the dependence is linear. It is important to stress that strong Coulomb correlations significantly reduce these crossover energies for a wide range of hole concentrations.[18] Thus the quadratic Fermi-liquid behavior[19] in the lifetime may, indeed, be "hidden" either by the limited resolution of the photoemission experiments or the "high" temperature onset of the normal state. In the present paper we relate the energy scales associated with the lifetime to those of the spin dynamics.

Our picture can be compared with alternative theoretical approaches to magnetic data. Recent Fermi-liquid-based schemes which have addressed NMR data all assume the existence of low-energy scales. In the "nearly magnetic" Fermi-liquid schools[20,21] these low energies arise from the proximity to an antiferromagnetic instability and are associated with soft spin fluctuation energies. In the "nearly localized" Fermi-liquid approaches,[17] such as that of Newns[12] and the present paper, the dominant near-instability results from proximity to a Mott localized insulator. Narrow bandwidths (which result from strong Coulomb correlations U), along with moderate spin fluctuation softening lead to low characteristic energies. It should be stressed that it is likely that both near magnetism and near localization are both playing a role in the metallic cuprates and it will be desirable eventually to treat these two near instabilities on a more even footing. In general the low energies discussed within these various approaches are of the order of a hundred or, at most, several hundred K, depending on the cuprate and its stoichiometry. Our detailed studies show that similar energy scales are also evident in neutron data on the Y-Ba-Cu-O system and we predict related effects in future neutron measurements of the La-Sr-Cu-O family.

Within the Fermi-liquid school, a phenomenological approach for understanding NMR data in the cuprates has been proposed by Millis, Monien, and Pines (MMP).[20] This picture assumes strong zone corner commensurate peaks in $\mathrm{Im}\chi(\mathbf{q},\omega\sim 0)$ for both Y-Ba-Cu-O and La-Sr-Cu-O and can explain quite well the T dependence of the (planar) Cu and O nuclear relaxations. However, the application of this phenomenology to recent neutron data[2-5] is not straightforward.

A related theory of Bulut, Hone, Scalapino, and N. E. Bickers[21] is based on the small Hubbard-U, RPA form for $\chi(\mathbf{q},\omega)$. While this theory has many similarities to the present approach, because it treats U as a small rather than large parameter, it leads to $\mathbf{q}$ structure in the spin dynamics which is different from that of the present theory. Stated simply, in the present paper we find that the spin exchange $J_H(\mathbf{q})$ appears in the same location within the RPA denominator as does the Hubbard U in the theory of Ref. 21. It will be seen that this $\mathbf{q}$ dependence in $J_H(\mathbf{q})$ plays a particularly important role in our work on the Y-Ba-Cu-O family. On the scale of the various theoretical scenarios for the high-temperature superconductors, differences between our picture and those of Refs. 20 and 21 are rather small. One should view the present approach and those of Millis, Monien, and

Pines[20] and Bulut, Hone, Scalapino, and Bickers[21] as belonging to the same general class of theories. Thus, much of the content of our paper, should, in principle, apply to the other two theoretical approaches, as well.

The above Fermi-liquid-based models for $S(\mathbf{q},\omega)$ should be contrasted with more localized (non-Fermi-liquid) schemes such as studies of the spiral phases.[22] Within the context of t-J and related models it is possible to explain the various commensurate and incommensurate structure observed in the neutron cross section. Here a long-range-ordered state is generally considered. It may be argued that fluctuation effects will destroy long-range order, leaving residual $\mathbf{q}$-structure peaks. However, at present, these theories appear to be inconsistent with the Fermi surfaces observed in photoemission experiments. Furthermore, within these approaches there is no strong *a priori* reason why the different cuprates would exhibit significantly different spin dynamics.

More generally the differences between the two cuprates appear to us to have no "natural" explanation except insofar as they correlate with the Fermi-surface shapes. When viewed in this way, as a form of Fermi-surface spectroscopy, these magnetic data take on an even greater significance. Just as in photoemission experiments, one may hope to test important features of the normal state, such as the nature and number of the spin and charge carriers, features of the energy band dispersion, as well as important energy scales and their hole concentration x dependence.

These detailed x-dependent neutron and NMR studies are now becoming available and they will provide crucial constraints for all normal-state theories. The present approach, which involves a Coulomb renormalized band structure, may be compared to the data as a function of x. In this context we address in detail two oxygen stoichiometries in the Y-Ba-Cu-O system, roughly corresponding to $O_{6.7}$ and O_7. In the La-Sr-Cu-O system we focus on two Sr concentrations, $x=0.09$ and $x=0.18$. In addition, we discuss the general functional form for a number of properties in this family, as well as the limiting value as $x\rightarrow 0$. Particularly interesting is the behavior of the incommensurability vector[5], $\delta(x)$, associated with the position of the peaks in the magnetic structure factor. Reasonably good agreement with recent measurements of this quantity provide support for the present approach in which the renormalized band parameters are found to vary as a function of the hole concentration x.

This paper is focused on numerically generated results for the dynamical structure factor as a function of $\omega, \mathbf{q}, T$ and x in the two cuprates. The formalism upon which this work is based is presented elsewhere.[14] Additional brief summaries of magnetic calculations are contained in Refs. 15 and 18 for the La-Sr-Cu-O system and Ref. 16 for Y-Ba-Cu-O. Here we concentrate on comparing the two cuprates and addressing recent neutron data and related energy scales. Among the important contributions of this paper are the following: (a) Insights into the quantitative behavior of the incommensurability in La-Sr-Cu-O. We show that the experimental result of Cheong *et al.*[5] $\delta\sim 2x$ requires the existence of a sizeable next-nearest-neighbor hopping term (nonzero, t_{pp}) in the Hamiltonian as well as a variation (with hole concentration x) in the Coulomb "renormalized" tight-binding Hamiltonian parameters. In this way neutron experiments may be seen to imply that the Fermi-surface shape (as well as its volume) depends on x. (b) The theoretical demonstration that a low-temperature crossover (from Fermi liquid T^2 to a high-temperature linear in T) dependence of the quasiparticle lifetime or resistivity also exists in the Y-Ba-Cu-O system. As in our previous studies of La-Sr-Cu-O,[18] this derives from the Van Hove energy scale, renormalized by Coulomb correlations. Here, however, the rotated band structure leads to a significantly higher Van Hove energy. (c) The observation that this "crossover" energy appears in the neutron data as a peak in $\mathrm{Im}\chi$ versus ω and thus is evident as a low-energy scale. This lends experimental support to the underlying assumption of Fermi-liquid-based approaches that such low energies do, indeed, exist. (d) The demonstration of similar crossover effects in the frequency dependence of the photoemission lifetime.[19] This observation along with (c) shows how the energy scales of the spin dynamics and quasiparticle lifetime are related. (e) The demonstration that including interlayer coupling within the unit cell of Y-Ba-Cu-O does not significantly change the character of the planar Lindhard function, so that simple one-layer calculations of this quantity are adequate for many purposes. (f) The presentation of predictions for the $(\mathbf{q},\omega,T)$ dependence of the neutron cross section in the fully oxygenated Y-Ba-Cu-O system, where experiments are just beginning[4] to reveal antiferromagnetic peak structure. In this paper we also address some aspects of ω/T scaling in the La-Sr-Cu-O system (which occurs along the zone diagonal direction) and touch on the role of the neutron and dc susceptibility "spin gap".[23,24] We note that these spin gap effects are not present, at least at the RPA level, in our calculations.

We now outline the remainder of the text. Section II presents the general formalism for calculating the dynamical susceptibility. In Sec. III, we present results for the $\mathbf{q}$ dependence of the neutron cross section in both the three-band (Sec. III A) and one-band (Sec. III B) cases. The present theory yields agreement with the wave vector $\mathbf{q}$ and temperature T dependence of $S(\mathbf{q},\omega)$ observed in Y-Ba-Cu-O as well as in La-Sr-Cu-O. Moreover, for the latter system our Coulomb renormalized band structure provides an explanation for the measured concentration dependence of the incommensurability vector. This situation is to be contrasted with the results obtained in the one-band models. Section IV focuses on the frequency and temperature dependence of the magnetic data. We emphasize that the various low-energy scales which appear in neutron experiments[3,4] on deoxygenated Y-Ba-Cu-O are consistent with the present theory. These energy scales, softened by spin-fluctuation effects, are related to the Van Hove singularity as well as the "coherence" temperature. (The latter temperature will be defined in more detail below). For the La-Sr-Cu-O system we present predictions regarding the frequency and temperature dependences of the maxima in $S(\mathbf{q},\omega)$. NMR experiments are discussed in Sec. V, where it is shown that the calculated Cu $1/T_1$ is consistent with the

data. By contrast, the standard hyperfine coupling model[20,21] for the oxygen relaxation does not lead to sufficient form factor cancellation effects to explain the difference between $1/T_1$ at the Cu and O sites in $YBa_2Cu_3O_7$. This imperfect cancellation derives from the fact that the antiferromagnetic peaks in the structure factor are not sufficiently sharp (as seems to be compatible with neutron-scattering observations[2-5]). In Sec. VI we discuss the results for the frequency and temperature dependence of the quasiparticle lifetime in $YBa_2Cu_3O_7$. These calculations lead to linear dependences on the relevant energy and demonstrate how the energy scales which appear in magnetic data are reflected in the lifetime. Furthermore, they lend support to the picture that the canonical Fermi-liquid quadratic (T,ω) dependences are "hidden" by the relatively high temperatures of the normal state (in resistivity data), or the limited frequency resolution (in photoemission data). Our conclusions are presented in Sec. VII.

II. GENERAL FORMALISM

A. Auxiliary boson scheme

We start from the extended three-band Hubbard Hamiltonian with large Cu on-site correlation U, which is reviewed in Ref. 17. Here we consider both the "electron" and "hole" pictures. These two descriptions are distinguishable only when $U\to\infty$. It is important to stress that the *physics* in the two pictures is equivalent, provided the Hamiltonian parameters are chosen to yield a Mott insulating state at half filling. Our formalism builds on the CuO_2 Hamiltonian written in the auxiliary boson basis

$$H=\sum_{i\sigma}\varepsilon_d^0 d_{i\sigma}^\dagger d_{i\sigma}+\sum_{l\sigma}\varepsilon_p p_{l\sigma}^\dagger p_{l\sigma}+\sum_{l_1 l_2\sigma}t_{pp}(p_{l_1\sigma}^\dagger p_{l_2\sigma}+\text{H.c.})+\sum_i\varepsilon_e e_i^\dagger e_i+\sum_i\varepsilon_f f_i^\dagger f_i$$
$$+\sum_{i,l,\sigma}V_{pd}[e_i d_{i\sigma}^\dagger p_{l\sigma}+f_i^\dagger d_{i-\sigma}p_{l\sigma}\mathrm{sgn}(\sigma)+\text{H.c.}]+\sum_i i\lambda_i\left[\sum_\sigma d_{i\sigma}^\dagger d_{i\sigma}+e_i^\dagger e_i+f_i^\dagger f_i-NQ_0\right], \tag{1}$$

where $e_i^\dagger$, $d_{i\sigma}^\dagger$, and $f_i^\dagger$ are the creation operators for the Cu^{1+}, Cu^{2+}, and Cu^{3+} valence states, respectively. The first and last of these correspond to bosons whereas the Cu^{2+} state is a fermion with specified spin index σ. This Hamiltonian is derived from the extended Hubbard Hamiltonian by representing a copper electron operator in terms of its valence state as $D_{i\sigma}^\dagger=d_{i\sigma}^\dagger e_i+\mathrm{sgn}(\sigma)d_{i,-\sigma}f_i^\dagger$. The energy to create a Cu^{1+} (no hole) state is $\varepsilon_e=0$, and that to create a Cu^{3+} state (two holes) is $\varepsilon_f=2\varepsilon_d^0+U$. In Eq. (1) a Lagrange multiplier $i\lambda_i$ is introduced to account for all possible valence states at each Cu so that $\sum_\sigma d_{i\sigma}^\dagger d_{i\sigma}+e_i^\dagger e_i+f_i^\dagger f_i=1=NQ_0$. In the context of a controlled $1/N$ expansion (where N is the Cu and O spin degeneracy), we choose $Q_0=1/N$ to be finite.

The Hamiltonian thus includes copper-oxygen hybridization V_{pd}, a finite oxygen dispersion derived from t_{pp} and oxygen and "bare" copper levels called ε_p and ε_d^0, respectively. In both cuprates we chose the band parameters so that there exists a Brinkman-Rice (or Mott localized) insulator at half filling. This Hamiltonian in the large-U limit can be solved[25] within a mean-field approximation[26,27] to produce a renormalized band structure which characterizes the quasiparticles of the Fermi liquid. In this limit the Lagrange multiplier and boson expectation values are replaced by (site-independent) scalars λ_0 and e_0, etc. and the renormalized d level position is $\varepsilon_d=\varepsilon_d^0+\lambda_0$. Finally the hybridization V_{pd} is renormalized as $V_{pd}\to V_{pd}^*$, which vanishes at the insulating limit as a consequence of large U. These various renormalizations are in the same spirit as the $m\to m^*$ renormalization of Landau theory. They may be viewed as the natural generalization of the result for isotropic Fermi liquids, to the multiband case. The quasiparticles are composed of hybridized copper and oxygen states with corresponding "weight" or coherence factors $u_{nr}(\mathbf{k})$ (where the index $n=1,2,3$ refers to one of the three renormalized bands and $r=d,p_x,p_y$ represents Cu or O sites). These coherence factors characterize the wave functions of the quasiparticles and are dominated by the Cu component. Because of strong Coulomb correlations, the renormalized antibonding band is greatly reduced in width and, as the insulator is approached becomes progressively more narrow.

Various schemes which go beyond the mean-field approximation (or leading order in $1/N$) have been presented in the literature.[17] These higher-order corrections are associated with the Landau parameters which describe the residual interactions between the quasiparticles of the renormalized band structure. The first-order corrections are of a "density-density" symmetry, so that spin-spin interactions do not appear until the $(1/N)^2$ level. These spin-spin terms were discussed in a previous paper[14] and lead to two types of contributions to the exchange interaction: superexchange and RKKY. It is important to stress that alternative schemes (e.g., perturbation in V_{pd}) give similar answers, so that our results are not artifacts of the $1/N$ expansion. Physically, these two types of exchange processes may be understood as deriving from Cu-Cu interactions via mediating oxygen states which are full (superexchange) and partially empty (RKKY).

The RKKY and superexchange contributions are both dependent on the occupation of the oxygen band. In this way, the value of the total exchange $J_H(\mathbf{q})$ depends on the hole concentration. The extreme limits of small and large t_{pp} are most readily amenable to quantitative discussion. We have shown,[14] that in the limit of large t_{pp} the RKKY interaction rapidly increases from zero with increasing x, whereas the superexchange term decreases with x. At larger values of the hole concentration the RKKY term dominates; it is initially ferromagnetic, and

ultimately antiferromagnetic with increasing x. By contrast, in the limit of small t_{pp}, the RKKY term is suppressed and the superexchange contribution becomes more dominant. In this case the net exchange $J_H(\mathbf{q})$ is more weakly dependent on the hole concentration. Because t_{pp} in the cuprates is neither very small nor very large, a quantitative calculation of the net exchange does not fall into either of the simple limiting cases. For this reason, we have appealed to phenomenology to treat the overall magnitude of the exchange which we parametrize by J_0. Comparison with NMR and neutron data seems to suggest unambiguously that this net exchange is antiferromagnetic in sign.

To estimate the $\mathbf{q}$ dependence we appeal to our numerical calculations[14] which have determined that the interaction is dominantly between nearest neighbors. We find these short-range exchange interactions occur (for both large and small values of t_{pp}) over the entire parameter regime in which the exchange interaction is dominated by the antiferromagnetic superexchange. This is an important consequence of strong Coulomb correlations which lead to quasilocalized Cu states. The strong on-site U terms are projected out so that the spin exchange is primarily between adjacent Cu atoms. To avoid further computational difficulties, we will approximate the $\mathbf{q}$-dependent exchange by a simple analytic expression (which corresponds to a nearest-neighbor tight-binding form)

$$J_H(\mathbf{q})=J_0[\cos(q_x a)+\cos(q_y a)] \ . \tag{2}$$

On the basis of phenomenology, we assume an antiferromagnetic $J_0>0$ having a magnitude which yields reasonable correspondence with the energy scales of the neutron data in $YBa_2Cu_3O_{6.7}$ and with the temperature at which the Cu NMR deviates from Korringa behavior in $La_{1.85}Sr_{0.15}CuO_4$. Thus in the former system we choose $J_0/J_c=0.7$ for the $O_{6.7}$ case and for the latter cuprates we take $J_0/J_c=0.8$ for $x=0.09$. These are our fitted parameters; we may then interpolate on the basis of our x-dependent calculations to find $J_0/J_c\sim 0.5$ for the $YBa_2Cu_3O_7$ and ~ 0.6 for $La_{2-x}Sr_xCuO_4$ at $x=0.18$. It should be noted that our results are not particularly sensitive to variations of order $\sim 20\%$ in these parameters. Here J_c is the value of J_0 at which the system is magnetically unstable.

We have also found that $J_H(\mathbf{q})$ is only weakly dependent on T and ω. Formally, this result derives from the fact that the magnetic interactions depend more on the high-energy than low-energy fluctuations (which are sensitive to the details of the renormalized band structure). Physically, this very weak T,ω dependence reflects the large characteristic energies of the mediating oxygen band which is relatively unaffected by the Coulomb or band narrowing effects associated with the Cu states.

Because of the structure of the spin-spin vertex function, we have shown[14] that the entire RPA series may be resummed. This is not generally the case for $\mathbf{q}$-dependent interactions. Similar results are found for the heavy fermion problem. The final expression for the dynamical susceptibility in the presence of exchange interactions is

$$\chi_{rr'}(\mathbf{q},\omega)=\chi^0_{rr'}(\mathbf{q},\omega)+\frac{\chi^0_{rd}(\mathbf{q},\omega)[-J_H(\mathbf{q})]\chi^0_{dr'}(\mathbf{q},\omega)}{1+J_H(\mathbf{q})\chi^0_{dd}(\mathbf{q},\omega)} \ . \tag{3a}$$

The Lindhard susceptibility components are

$$\chi^0_{rr'}(\mathbf{q},\omega)=\frac{1}{N_{\rm site}}\sum_{nm\mathbf{k}}\frac{f(E_n(\mathbf{k}))-f(E_m(\mathbf{k}+\mathbf{q}))}{\omega-[E_n(\mathbf{k})-E_m(\mathbf{k}+\mathbf{q})]}u^*_{mr}(\mathbf{k}+\mathbf{q})u^*_{nr'}(\mathbf{k})u_{mr'}(\mathbf{k}+\mathbf{q})u_{nr}(\mathbf{k}) \ , \tag{3b}$$

where $E_n(\mathbf{k})$ are the renormalized quasiparticle energies reviewed in Ref. 17. In the limit $t_{pp}=0$, a compact analytical expression may be written for this dispersion

$$E_{1,\mathbf{k}}=\frac{\varepsilon_p+\varepsilon_d}{2}+\left[\left[\frac{\varepsilon_p-\varepsilon_d}{2}\right]^2+e_0^2\gamma_{\mathbf{k}}^2\right]^{1/2} , \tag{4a}$$

$$E_{2,k}=\frac{\varepsilon_p+\varepsilon_d}{2}\left[\left[\frac{\varepsilon_p-\varepsilon_d}{2}\right]^2+e_0^2\gamma_{\mathbf{k}}^2\right]^{1/2} , \tag{4b}$$

and

$$E_{3,\mathbf{k}}=\varepsilon_p \ , \tag{4c}$$

where e_0 is the mean-field value of the Cu^{1+} boson amplitude and $\gamma_k=2V_{dp}[\cos^2(k_x a/2)+\cos^2(k_y a/2)]^{1/2}$. Here the index $n=1,2,3$ corresponds to the antibonding, bonding, and nonbonding bands, respectively. More generally, however, the dispersion relations, which arise from the diagonalization of a 3×3 matrix, are rather complex[16] and will not be written down here. It should be stressed that the band parameters in Eqs. 4 are x dependent as a result of our self-consistent mean-field approach.

It is useful to summarize the present results for the dynamical susceptibility [Eq. (3)]. To leading order, the large Coulomb correlations are absorbed into the Lindhard term which derives from the narrow quasiparticle band. Interactions between the quasiparticles $J_H(q)$ arise from higher-order effects which can be systematized in the context of a $1/N$ expansion.[14]

We may compare and contrast the present model of Eq. (3) with the results of Ref. 21. Here the dynamical susceptibility is derived in the strong-U limit, using a Coulomb renormalized band structure and residual exchange interaction J_H. We will see that low-energy scales result from a combination of narrow band and spin-fluctuation softening. In Ref. 21 the corresponding calculation was presented for the weak-U limit. The authors of Ref. 21 view the cuprates as being very close to a magnetic instability so that the soft energies result entirely

from spin-fluctuation effects via a near instability of the RPA denominator $1-U\chi^0$. This corresponds to a "nearly magnetic" Fermi-liquid picture, as distinguished from the present "nearly localized" approach. In reality the truth may lie somewhere in between the two pictures and it is likely that both near localization and near magnetism are playing a role in the cuprates (as well as in other strongly correlated systems[17]).

Despite these differences, the general *form* for the dynamical susceptibility used in Ref. 21 is similar to that obtained in the present approach. This similarity in form is also seen in comparisons with the phenomenological approach of Millis, Monien, and Pines.[20] In this way, Eq. (3) may be considered to be a natural generalization to arbitrary $(\mathbf{q},\omega)$ of the standard Fermi-liquid result.

B. Phenomenological approach to renormalized band structure

In order to acquire additional intuition about the effects of strong Coulomb correlations on the Lindhard function $\chi^0(\mathbf{q},\omega)$, in this section we consider an alternate approach. Throughout this paper we will argue that the auxiliary boson scheme should be viewed as a convenient theoretical "tool" for incorporating band narrowing effects associated with strong U. In no sense is this scheme unique and similar results may be found within an alternate Gutzwiller approach.[28] Thus the conclusions of the present paper are not, in detail, sensitive to the use of this particular theoretical device.

To establish greater generality of the present physical picture, we consider a more phenomenological approach to the auxiliary boson scheme in which band narrowing effects are introduced by fits to the measured Drude plasma frequency $\omega_p^2 - n/m^*$. It should be stressed that this quantity is strongly hole concentration dependent and ω_p^2 vanishes linearly with x as $x \to 0$. In Fermi-liquid schemes the effective carrier number n is constrained by Luttinger's theorem to be nonzero above, but near the metal insulator transition. Thus the behavior of the plasma frequency represents an important constraint on m^* or the bandwidth. Alternate measures of this quantity involve thermodynamic variables such as the static susceptibility or specific heat, both of which contain important contributions from degrees of freedom unrelated to the conduction electron states. These additional contributions must be subtracted out in some approximate manner to estimate the renormalized electronic mass. Furthermore, because ω_p is temperature independent, it represents a less ambiguous measure of m^* than, say, the static susceptibility, which is T dependent for most hole concentrations.

The inset to Fig. 1 shows the measured behavior of the Drude-fitted[29,30] ω_p as a function of hole concentration in both families of cuprates. Here, in order to show the Y-Ba-Cu-O and La-Sr-Cu-O data on the same figure we have estimated the hole concentration in the former (assuming O_7 corresponds to $x=0.33$ and that the chains and planes share the holes in a 1:2 ratio). This assigned hole concentration is viewed as only semiquantitative. In the main body of the figure we show the plasma frequency which is derived from our auxiliary boson calculation of the renormalized band structure for the Y-Ba-Cu-O family. Here the parameters are chosen to be those used throughout the paper for the spin dynamical calculations. In this way the energy scales associated with structure in $\chi^0(\mathbf{q},\omega)$ are compared with the band energy scales measured in the plasma frequency. This figure indicates that the band narrowing effects of the present strong-U theory correspond to those determined from the measured plasma frequency. Equally important, as the insulator is approached $\omega_p^2 \to 0$ as a consequence of the vanishing of the renormalized hybridization V_{pd}^*. This behavior reflects the growing localization of the Cu states. It demonstrates how the Fermi-liquid state breaks down as the insulator is approached.

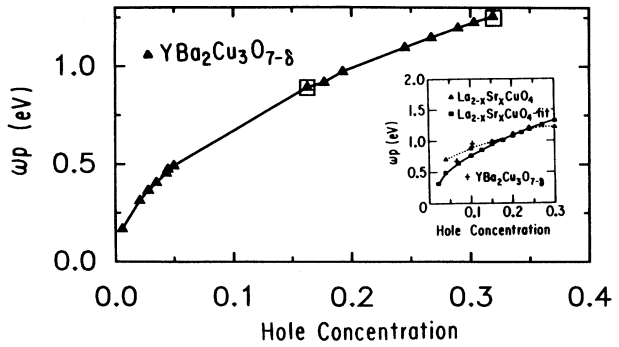

FIG. 1. Calculated plasma frequencies ω_p of $YBa_2Cu_3O_{7-\delta}$ as a function of hole concentration (estimated as in text). The two points surrounded by squares represent $YBa_2Cu_3O_{6.7}$ and $YBa_2Cu_3O_7$ with the same parameters used in the spin dynamical calculations. The inset shows (Drude) measured ω_p of the two indicated cuprates (Refs. 29 and 30), where the "fitted" curve is drawn through three x values (near optimal concentration) to represent $\omega_p \propto x^{1/2}$.

The above observations suggest an alternative, more phenomenological approach to incorporate strong-U effects. Rather than use the auxiliary boson scheme as our starting point, we have found that similar results for the spin dynamics obtain if we take the *ratios* of the tight-binding band parameters from, say, the LDA scheme and *fit* their overall energy scale to the measured plasma frequency. In this way the band shapes are constrained via LDA calculations or angle-resolved photoemission experiments while the bandwidths narrow in a fashion dictated by the plasma frequency. Such a phenomenological approach implicitly includes a tendency towards Cu localization and thus incorporates the eventual breakdown of the Fermi-liquid state in much the same way as the auxiliary boson scheme.

III. THE q DEPENDENCE OF THE NEUTRON STRUCTURE FACTOR

A. Three-band models for Y-Ba-Cu-O and La-Sr-Cu-O

In the Y-Ba-Cu-O system LDA calculations indicate that the Fermi-surface shape is rotated by 45° relative to that predicted from a nearest-neighbor, tight-binding scheme.[7] By contrast these same calculations indicate

that in the La-Sr-Cu-O family[10] the Fermi surface corresponds rather well to a CuO_2 layer in which both nearest-neighbor (Cu-O) and next-nearest-neighbor (O-O) hopping processes are included. In this way the Fermi surface is represented by the diamondlike shape slightly modified by these higher-order hopping processes.[31] [A plot of this Fermi surface is shown in Fig. 2(a)]. It follows, then, that the two cuprates have Fermi surfaces which are, roughly, related by a 45° rotation. As will be emphasized throughout, this rotation leads to very different nesting structure, which in turn is reflected in the $\mathbf{q}$ dependence of $S(\mathbf{q},\omega)$.

This rotation has been most extensively discussed in Ref. 9. There it is claimed to be associated with the hybridization between the apical oxygen and the planar Cu and appears to persist throughout the range of metallic oxygen concentrations.[8] We are not aware of any tight-binding parametrization in the theoretical literature for describing the planar bands of Y-Ba-Cu-O within the usual three-band model. The present calculations determine these parameters on phenomenological grounds. Here we model this band structure by including second-nearest-neighbor oxygen-oxygen[32] overlap integrals (via t'_{pp}) in the tight-binding Hamiltonian of Eq. (1). In principle, these may be viewed as arising via O_4-O_2 interactions.

Figures 2(a) and 2(b) correspond to the Fermi surfaces

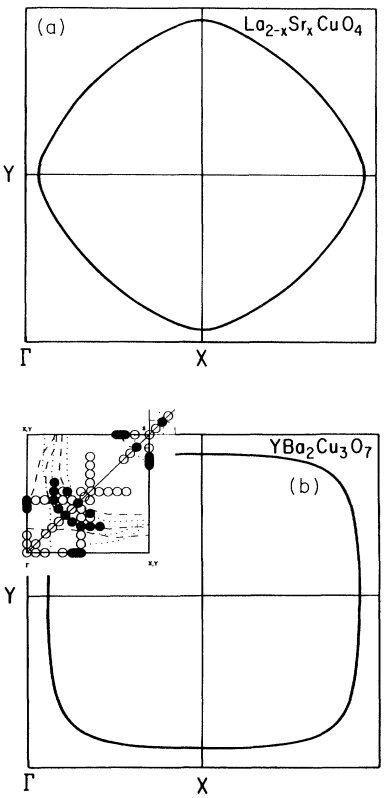

FIG. 2. Calculated Fermi surface using present strong-U theory for (a) $La_{1.85}Sr_{0.15}CuO_4$ and (b) $YBa_2Cu_3O_7$. The inset shows the measured (solid circles, Ref. 6) and LDA-calculated (dashed lines, Ref. 7) Fermi surface for $YBa_2Cu_3O_7$.

of $La_{2-x}Sr_xCuO_4$ with $x=0.18$ and $YBa_2Cu_3O_7$, respectively, which are derived from the Hamiltonian of Eq. (1), solved within the mean-field approximation and using the following parametrizations. For the La-Sr-Cu-O family we chose the parameters such that (in the "hole" picture) $\varepsilon_p-\varepsilon_d^0=4$ eV, $V_{pd}=0.6$ eV, and the (nearest-neighbor) oxygen-oxygen overlap $t_{pp}=-0.2$ eV. Similarly, for this case we also studied the electron picture with $\varepsilon_p-\varepsilon_d^0=4$ eV, $V_{pd}=1.6$ eV, and $t_{pp}=0.4$ eV. The latter parametrization is reasonably consistent with *ab initio* values in the literature,[33] whereas the former requires a smaller value of the Cu-O overlap in order to produce the Mott insulating state at half filling.[17] Unless indicated otherwise, all results presented in this paper are insensitive to which of the two pictures is used (within factors of order unity). For definiteness, all figures are based on the first parametrization. For the Y-Ba-Cu-O family we did not explore the two alternate descriptions in as much detail and here describe results for the electron picture. However, based on our experience with La-Sr-Cu-O, a hole-based approach would lead to equivalent results.

In Y-Ba-Cu-O, to achieve the Fermi-surface rotation, we included both first- and second-neighbor oxygen-oxygen overlaps called, respectively, t_{pp} and t'_{pp}. In order to obtain reasonable agreement with the measured (and calculated) Fermi-surface shape, we chose $V_{pd}=1.29$ eV, $\varepsilon_p-\varepsilon_d^0=5$ eV, and $t_{pp}=1.2$ eV and $t'_{pp}=-1.0$ eV. Slightly smaller values of these last two parameters can also be used to effect the rotation ($t_{pp}=0.9$ eV and $t'_{pp}=-0.6$ eV) although the shape of the calculated Fermi surface at Γ better matches that deduced experimentally in the first case. For that reason we focused on this first parametrization. One may view the relatively large oxygen-oxygen overlap parameters as simulating more extended hopping processes, which are truncated in the usual tight-binding scheme.

It should be noted that in our large-U formalism, the dominant contribution to the Lindhard function comes from planar Cu d electrons, while the Fermi-surface rotation is effected through higher-order oxygen hopping processes. In this way we have essentially separated the states which are responsible for the spin dynamics from those which lead to the rotation of the Fermi surface. As will be shown in more detail below, numerical calculations establish that the Lindhard function depends most strongly on the shape of the Fermi surface and is less sensitive to the detailed parametrization which we have invoked to fit the fermiology.

For definiteness, in the Y-Ba-Cu-O family we take the hole concentration x to be 0.18 in order to simulate the $O_{6.7}$ cuprate and $x=0.36$ to correspond to O_7. The precise values of x are difficult to determine at this stage particularly since there is likely to be plane-chain charge transfer in this system.[34] We note that the energy scales which will be presented below are not in detail sensitive to variations in x, within the physical range of doping concentrations. For ease in comparison we show in the inset of Fig. 2(b), the measured[6] (dark circles) and LDA calculated[10] (dotted and dashed lines) planar Fermi surfaces for $YBa_2Cu_3O_7$. Agreement between these photoemission data and conventional band calculations is

surprisingly good. It should be noted from the inset that there are actually two planar bands corresponding to the two CuO_2 layers within the unit cell of Y-Ba-Cu-O. Interactions between these layers break the degeneracy of the bands. Because of the obvious complexity we will for the most part, treat these bands as degenerate. However, we briefly present results for the Lindhard function contribution for a two-layer system.

Given the band structure, the Lindhard functions can be calculated in a straightforward manner. Our numerical algorithms are based on a two-dimensional generalization of the standard three-dimensional tetrahedral method. The latter has been used previously[35] to address the neutron-scattering cross section in heavy fermion metals.

The calculated structure factor $S(\mathbf{q},\omega)$ as a function of q_x and q_y is shown for the La-Sr-Cu-O system in Figs. 3(a) and 3(b) for $x=0.09$ and $x=0.18$, respectively. Here the temperature is 1 meV and the frequency $\omega=10$ meV. It should be stressed that while Figs. 3(a) and 3(b)

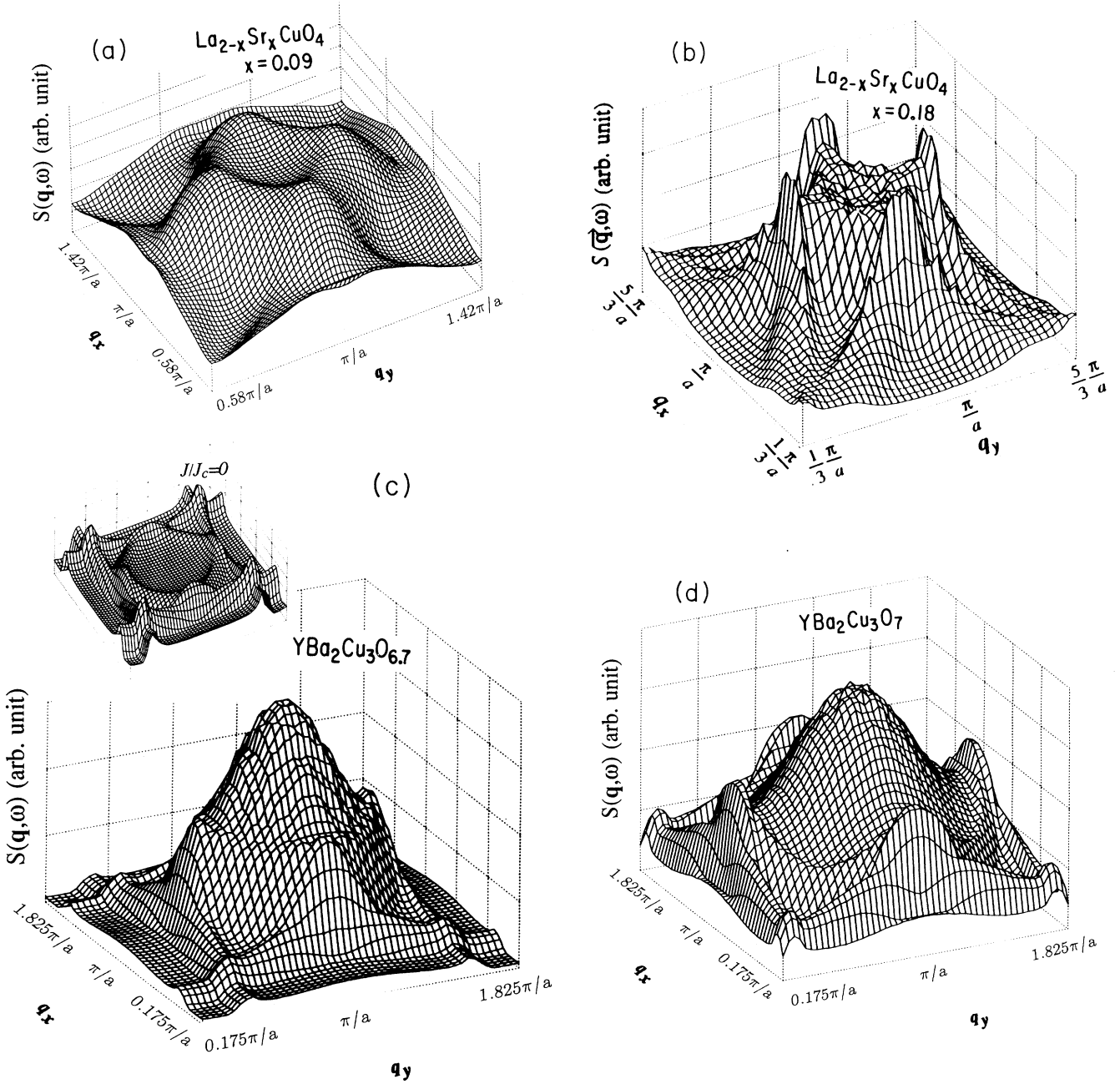

FIG. 3. Plots of $S(\mathbf{q},\omega)$ vs (q_x,q_y) for $La_{2-x}Sr_xCuO_4$ at (a) $x=0.09$ and (b) $x=0.18$, and for $YBa_2Cu_3O_{6.7}$ (c) and $YBa_2Cu_3O_7$ (d). Here the temperature and frequency are 1 and 10 meV, respectively, and the inset in (c) plots the Lindhard function ($J_0=0$) contribution for the same range of (q_x,q_y).

contain the effects of nonzero spin exchange $J_H(\mathbf{q})$, the general shape of $S(\mathbf{q},\omega)$ is the same with and without J. This is a consequence of the detailed fermiology and results from the fact that there is considerable structure in $\mathrm{Im}\chi^0(\mathbf{q},\omega)$ around the $\mathbf{Q}_0=(\pi/a,\pi/a)$ point. It is common in the Y-Ba-Cu-O literature to use an alternate notation for $\mathbf{Q}_0=(\frac{1}{2},\frac{1}{2})$ in terms of reciprocal lattice units (r.l.u.). We will use both of these conventions interchangeably here. At this value of $\mathbf{q}=\mathbf{Q}_0$, $|J_H(\mathbf{q})|$ also has a maximum, but it is still smoothly varying on the scale of the Lindhard contribution. Consequently the spin-spin interaction terms enhance the overall magnitude of $S(\mathbf{q},\omega)$ near $\mathbf{Q}_0$, but do not change its shape.

For both concentrations, the structure around the $\mathbf{Q}_0$ point consists of four maxima along the four corners of a square, with a minimum of $\mathbf{Q}_0$.[36] For the higher x value this incommensurate structure near $\mathbf{Q}_0$ contains a mix of two components which we characterize as the "band-structure" singularity term and the "nesting" contribution. The latter is associated with a dynamical Kohn anomaly (related to the two-dimensionality) and enhanced by nesting. It may be seen quite generally that for some values of $\mathbf{q}$ there will be singular contributions to $S(\mathbf{q},\omega)$ arising from the two-dimensional (2D) tight-binding band structure. These terms, which appear as spikes in Fig. 3(b) are reminiscent of the 2D Van Hove singularity in the (one-particle) density of states, and may be traced to the delta-function contribution $\delta(E_n(\mathbf{k}+\mathbf{q})-E_n(\mathbf{k})+\omega)$ to $\mathrm{Im}\chi^0(\mathbf{q},\omega)$. In this way, they represent singularities in the "two-particle" density of states. The Fermi-function contributions which multiply these terms in Eq. (3b) give rise to the nesting component. The band-structure singularities are temperature *independent,* whereas the nesting features are not. Thus the former remain strong (although reduced in amplitude) with increasing temperature. Inclusion of lifetime effects will, however, lead to some T suppression of these and other peak structures. Furthermore, we find that these singularity terms are sensitive to the details of the band structure and, for different parametrizations, need not be as close to the Kohn anomaly contributions as shown in the figure.

The relative position of the two contributions to $S(\mathbf{q},\omega)$ changes significantly with x, primarily as a result of the changes in the nesting vectors. In the case of Fig. 3(a), because x is sufficiently small, the band-structure singularity does not significantly overlap the nesting features, so that it is not visible on the scale of the figure. In this case, structure around $\mathbf{Q}_0$ derives entirely from nesting. At the higher value ($x=0.18$) of Fig. 3(b), the four "spikes" associated with the singularity are clearly visible and nearly overlap the nesting contribution. At still higher x the relative position of the two contributions is inverted and the singularity structure dominates the topography around $\mathbf{Q}_0$.

A similar competition between nesting and 2D band-structure singularity contributions may be seen in the Lindhard function of the Y-Ba-Cu-O family. This Lindhard contribution to $S(\mathbf{q},\omega)$ is plotted in the inset of Fig. 3(c) for the $O_{6.7}$ case. Because of the 45° rotation of the Fermi surface, there is no nesting structure associated with the $\mathbf{Q}_0$ direction. This is in clear contrast to the results of Figs. 3(a) and 3(b) which indicate that La-Sr-Cu-O (unlike Y-Ba-Cu-O) has a clear predisposition towards these $\mathbf{Q}_0$ "antiferromagnetic" peaks arising from its Fermi-surface shape. In Y-Ba-Cu-O, as shown in the inset, nesting leads to the inner and outer ridge structures, whereas the band-structure singularity gives rise to other peaks along $q_x\sim 0$ or $q_y\sim 0$, which are located beyond the range of the figure.

In striking contrast to the case of zero $J_H(\mathbf{q})$, is the behavior for physical values of the exchange interaction. The main portion of Fig. 3(c) shows the effects of finite $J_H(\mathbf{q})$ in $YBa_2Cu_3O_{6.7}$. Because of the relatively flat topography of the Lindhard function around the $(\pi/a,\pi/a)$ point, when finite J is included in the spin dynamics, it produces a (commensurate) maximum at $\mathbf{Q}_0$. This peak directly reflects the $\mathbf{q}$ dependence of $J_H(\mathbf{q})$ of Eq. (2). Similar effects are seen in Fig. 3(d) for the YBa_3CuO_7 system. These figures will be discussed in the context of more detailed experimental comparisons later in this section. Nevertheless, it should be noted here that the present calculations can provide an explanation for the observed[2,5] incommensurate peak structures in La-Sr-Cu-O, with associated temperature dependent widths, and the commensurate peaks[3,4] in Y-Ba-Cu-O (at reduced oxygen stoichiometries) with *temperature-independent* magnetic correlation lengths. The former arise from the details of the Fermi-surface shape, the latter from the $\mathbf{q}$ dependence of the exchange interaction.

While we have emphasized the one CuO_2 layer model thus far, the unit cell in Y-Ba-Cu-O actually consists of two interacting layers. Evidence for electronic coupling of the bilayers is provided by photoemission data which are indicated in the inset of Fig. 2(b). This electronic coupling is also present in the LDA-derived band structure, also shown in the inset. It is therefore clear that a full calculation of this Lindhard function should include the bilayer coupling. Because a full bilayer, multiband renormalized band structure is difficult to implement, here we consider a slightly oversimplified model in order to illustrate the effects (of bilayer coupling only) on the Lindhard function χ^0. This discussion is included primarily to justify the one-layer approximation to the Lindhard function by showing that there are no qualitative changes in the contribution of the CuO_2 planes as a result of interlayer coupling. The important effects of interlayer magnetic correlations have been discussed by Zha, Si, and Levin[16] and are essential to include, if one is to understand the observed q_z modulation[3] in this cuprate. We have found that $\chi^0(\mathbf{q},\omega)$ is more sensitive to the *shape* of the Fermi surface than to the details of the parametrization; therefore, we believe the one-band model is adequate for our purposes.

Here we consider a two-layer tight-binding model which is assumed to contain only one species of atoms. In this case the electronic dispersion is given by

$$E_{1,\mathbf{k}}=\varepsilon-2t_1(\cos k_x a+\cos k_y a)+4t_2\cos k_x a\cos k_y a+2t_3, \tag{5a}$$

$$E_{2,\mathbf{k}}=\varepsilon-2t_1(\cos k_x a+\cos k_y a)+4t_2\cos k_x a\cos k_y a-2t_3, \tag{5b}$$

where t_1 and t_2 are the first- and second-nearest-neighbor hopping terms between atoms in each layer, respectively, and t_3 the hopping term between two atoms in different layers. We chose the parameters $t_1=0.25$ eV, $t_2=0.125$ eV, $t_3=0.04375$ eV, and the Fermi energy $E_F-\varepsilon_p=-0.2875$ eV in order to match the Fermi-surface shape with that deduced experimentally. The resulting Fermi surfaces, shown in the inset of Fig. 4 have a splitting which is in reasonable agreement with what is expected on experimental grounds. [See inset of Fig. 2(b)].

The Lindhard function for this case (corresponding to the experimentally deduced Fermi surfaces in the fully oxygenated limit) is plotted in the main portion of Fig. 4. Comparison with the inset of Fig. 3(c) indicates that there are no qualitative differences. The slightly smaller volumes of the two Fermi surfaces shift the inner ridge structure towards $\mathbf{Q}_0$, relative to the one-layer case shown in the inset.[37] Thus for physical values of the interlayer hopping, our results for the $J_H(\mathbf{q})=0$ case are well represented by a one-layer model. It is reasonable to assume that this situation also persists in the presence of $J_H(\mathbf{q})$, although here it will be important to include the strong interlayer antiferromagnetic coupling discussed in Ref. 38 and in Ref. 16 by Zha, Si, and Levin.

We turn now to studies of various projections of these 3D plots along both the directions containing the peak maxima and along other symmetry points. The calculations in these plots can be more directly compared with experiment for the two cuprates, since the counterpart of the full 3D plots has not yet been obtained experimentally. A plot of the structure factor corresponding to Fig. 3(a) along the zone diagonal direction is shown by the upper panel in Fig. 5(a). The lower panel presents a projection of the 3D plot which intersects two of the four maxima on the figure. In both panels the top curves correspond to a temperature $T=1$ meV and the bottom to $T=10$ meV. To specify our coordinate system we define the vector $(\kappa_x,\kappa_y)=(q_x+\delta/2,q_y-\delta/2)$, where $\delta=0.18$ measures the incommensurability of the wave vector at which the structure factor is a maximum. The maximum wave vector thus corresponds to $((1\pm\delta)\pi/a,\pi/a)$ and $(\pi/a,(1\pm\delta)\pi/a)$. It may be seen that the nesting structure is relatively similar in the two directions.

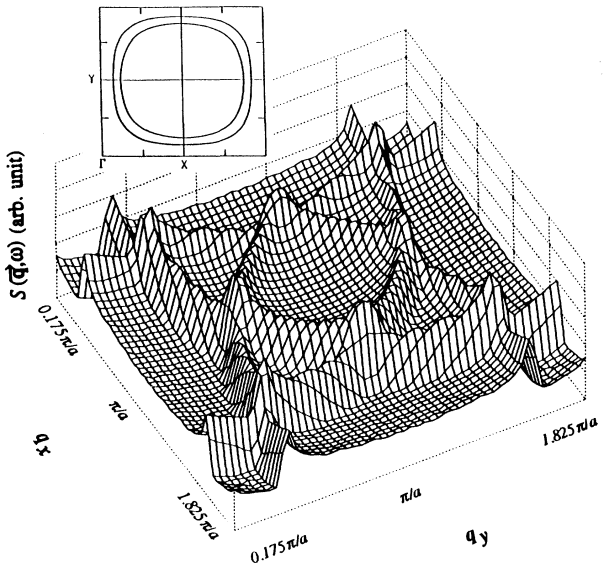

FIG. 4. Plot of Lindhard contribution to $S(\mathbf{q},\omega)$ vs (q_x,q_y) at $q_z=\pi$ for the two CuO_2 layer described in the text. Associated Fermi surfaces are shown in the inset.

By contrast the same plot for $x=0.18$ in Fig. 5(b) shows that the zone side peaks are higher and the minimum clearer than the counterparts in the diagonal plot. Here the zone side (κ,κ) direction intersects the band-structure singularity contributions, which were discussed above. It is these terms which yield sharp spikes in $S(\mathbf{q},\omega)$. Furthermore, the minimum at the $\mathbf{Q}_0$ point is deeper. In this case, the incommensurate wave vector corresponds to $\delta=0.33$. It may be seen that the effects of temperature are different in the two directions. The sharp peaks are not affected by thermal smearing as shown in the lower panel, whereas the diagonal peaks become unresolvable, at the higher temperature.

It should be noted that three-dimensionality as well as quasiparticle lifetime effects[39] along with finite instrumental resolutions will lead to a considerably broadened structure in any real experiment. Furthermore, because of the temperature dependence of the lifetime, $(-\mathrm{Im}\Sigma\sim T)$, it is likely that the sharp singularity structure will be progressively broadened as temperature increases. When these effects are included, our temperature-dependent results can be brought into reasonable agreement with recent data reported by Cheong *et al.*[5] Furthermore, as will be discussed later, the magnitude of the incommensurability as well as its x dependence is also consistent with these experiments.

We turn now to similar projections of the 3D structure factor for the Y-Ba-Cu-O system. Here, also, the upper and lower panels correspond to diagonal and off-diagonal plots. The temperature is taken as 1 and 11 meV for the upper and lower of each pair of curves within a panel. The diagonal plots in Fig. 5(c) correspond to $YBa_2Cu_3O_{6.7}$. Here it may be seen that the half width $(\Delta q=0.22)$ is rather large and essentially T independent. This follows from the fact that the peak around $\mathbf{Q}_0$ derives from the $\mathbf{q}$ dependence of $J_H(\mathbf{q})$, which was discussed in Eq. (2). This exchange interaction was found in our calculations[14] to be relatively T independent. The smaller side peaks shown at lower temperatures are related to nesting and disappear as expected upon heating. The off-diagonal plots shown in the two lower panels correspond to $S(\mathbf{Q}^*,\omega)$ along the $\mathbf{Q}^*=(\frac{1}{2},K)$ direction. Here, too, the subsidiary peaks are T dependent and thus related to nesting.

Similar studies of the fully oxygenated case are shown in Fig. 5(d). In the diagonal direction, the half width $\Delta q\sim 0.3$ is larger than in the $O_{6.7}$ case, although it is similarly T independent. All subsidiary maxima are nesting effects. Plots of the $\mathbf{Q}$ dependence along the $\mathbf{Q}^*=(\frac{1}{2},K)$ direction are shown in the lower panels. In this off-diagonal direction all secondary maxima shown in the figure are also consequences of nesting. For this (rotated) Fermi surface, the band-structure singularity effect

(similar to that discussed above for the La-Sr-Cu-O family) is associated with q_x or $q_y=0$. These effects are not visible on the scale of Figs. 5(c) and 5(d).

Because of the reduction in overall amplitude of the neutron-scattering intensity in the fully oxygenated case, (relative to $O_{6.7}$), these figures, as a whole, suggest that the O_7 **q** structure may only be seen with some difficulty.[40] Evidently, reductions in peak intensity of a factor of 2 may make this peak structure difficult to observe. We estimate, that even with a slightly larger J_0 it is unlikely that this reduction will be less than a factor of 2.

B. Comparison with one-band models: Incommensurability effects

In order to assess the generality of our results we have also considered some simple one-band (one-layer) Hubbard models, with and without next-nearest-neighbor hopping t_2. Variations in this latter parameter, along with variations in the hole concentration x, enable us to simulate the quasirealistic Fermi surfaces of Figs. 2(a) and 2(b) for the La-Sr-Cu-O and Y-Ba-Cu-O systems. It is important to stress, however, that the present approach introduces (Coulomb renormalized) tight-binding parameters which are dependent on the hole concentration x. Thus a fit to the one-band models necessarily implies that the various hopping parameters are also x dependent. In this section, we will monitor how changes in the fermiology lead to changes in the Lindhard function with particular emphasis on the incommensurability vector in La-Sr-Cu-O systems. In addition to studying the **q** structure in $\chi^0(\mathbf{q},\omega)$, we will also compare the effects of a **q**-dependent J on $S(\mathbf{q},\omega)$ with those deriving from the **q**-independent Coulomb parameter U. The latter replaces $J_H(\mathbf{q})$ in Eq. (3a) (and its one-band generalization), in the standard RPA theory.[21] Finally, we address the comparison between energy scales of the one-band RPA theory and the present three-band, Coulomb renormalized, strong-U approach.

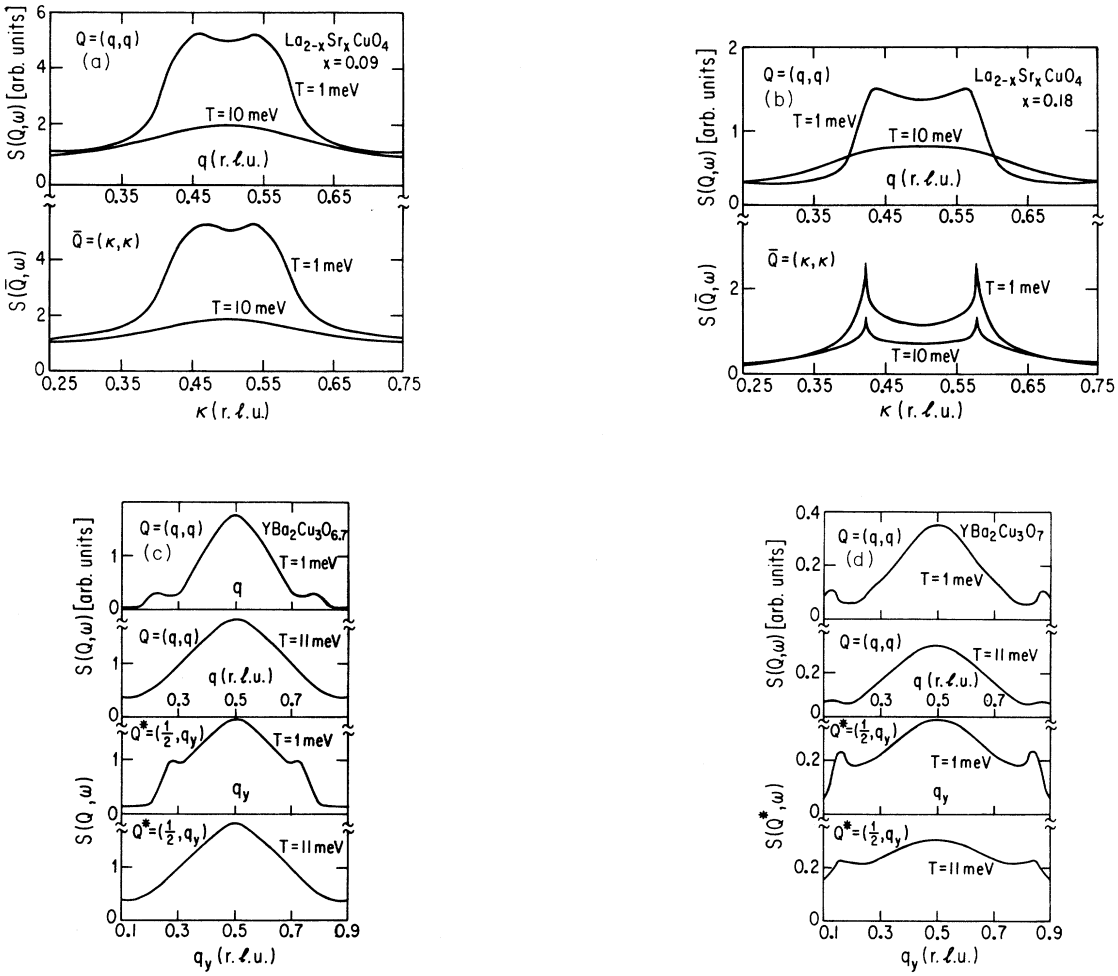

FIG. 5. Wave-vector dependence of the structure factor at $\omega=10$ meV, and for low ($T=1$ meV) and moderate ($T=10$ meV) temperatures. The upper and lower panels in (a) and (b) correspond to the diagonal and off-diagonal [intersecting the absolute maxima in $S(\mathbf{q},\omega)$] scans for $x=0.09$ and $x=0.18$, respectively. Similar diagonal [$\mathbf{Q}=(q,q)$] and off-diagonal $\mathbf{Q}^*=(\frac{1}{2},q_y)=(\pi/a,q_y)$ scans are shown for the Y-Ba-Cu-O system in (c) and (d).

We have reproduced the three-band-calculated shapes of the Fermi surface in both cuprates within the one-band models at each x value. Rather large values of $t_2/t_1=0.5$ are needed to obtain the rotated Fermi surface of $YBa_2Cu_3O_7$. Here t_1 is the nearest-neighbor hopping matrix element. For $t_2/t_1=0.25$, the Fermi surface of the Hubbard model with $x=0.18$ reproduces quite well the La-Sr-Cu-O three-band results of Fig. 2(a).

It is important to stress that in the La-Sr-Cu-O system, once the Fermi-surface shape is properly matched, both the one-band and three-band models yield a similar $\mathbf{q}$ structure in the neutron cross section. Thus the shape of the structure factor shown in Figs. 3(a) and 3(b) is "generically" associated with the usual cuprate (diamondlike) Fermi surface, seen in Fig. 2(a). This follows because the $\mathbf{q}$ dependence in $S(\mathbf{q},\omega)$ is dictated primarily by the Lindhard function. The effects of the RPA denominator $[1-U\chi^0(\mathbf{q},\omega)]$ or its counterpart in the three-band model $[1-J_H(q)\chi^0(\mathbf{q},\omega)]$ do not change the shape of the dynamical structure factor, only the peak height. By contrast in the Y-Ba-Cu-O system, the two models give very different results, even when the Fermi-surface shape is constrained to be the same. In the present, three-band case, commensurate peaks at $\mathbf{Q}_0$ appear in $S(\mathbf{q},\omega)$ as a consequence of the $\mathbf{q}$ dependence of the exchange interaction $J_H(\mathbf{q})$. In the one-band case, the RPA denominator introduces no new $\mathbf{q}$ dependences and the entire $\mathbf{q}$ structure in the cross section is dictated by the Lindhard function. Consequently in the one-band RPA-Hubbard model, with the rotated Y-Ba-Cu-O Fermi surface, one would have difficulty explaining the existence of antiferromagnetic peaks.

In the remainder of this section we concentrate on the La-Sr-Cu-O family where the one- and three-band models are reasonably similar. We address both the relevant frequency scales as well as the x dependence of the incommensurability vector. It is clear that even though the $\mathbf{q}$ dependence can be made to coincide, the dynamical energy scales have a different origin. In the one-band Hubbard, RPA approach[21] to obtain the characteristic low-energy scales observed in the spin dynamical experiments, it is important to include the RPA (denominator) contribution to $\chi(\mathbf{q},\omega)=\chi^0(\mathbf{q},\omega)/[1-U\chi^0(\mathbf{q},\omega)]$. In this way when the maximum of $U\chi^0(\mathbf{q},0)$ is chosen to be close to unity, the antiferromagnetic spin fluctuations will be sufficiently soft to explain the low-energy scales ($\sim$10–20 meV) seen in NMR and neutron experiments. By contrast in the present approach, narrow bandwidths combined with antiferromagnetic spin fluctuations of *moderate* strength can produce these same low-energy scales.

Comparison of the x-dependent incommensurability vector in the one- and three-band approaches yields a further important difference. Without a Coulomb renormalization of the band parameters (with x), the incommensurability vectors in the one-band case are only weakly x dependent. This leads to inconsistencies with the experimental observation that

$$\delta(x)\sim 2x \ . \tag{6}$$

More specifically, in the presence of a nonvanishing t_2 term, the $x=0$ point plays no special role. For this reason the incommensurability is expected to remain nonzero at $x=0$.[41] This situation is to be contrasted with the limit $t_2=0$. Here, perfect nesting at half filling leads to a vanishing of $\delta(x)$ at this point. While this feature is in agreement with experiment, when $t_2=0$, the size of the incommensurability is too small to explain the data away from $x=0$. Indeed, the $t_2=0$ case has the wrong Fermi-surface curvature to be consistent with the sign of the Hall effect.[16] For this reason, even if spin dynamical data were unavailable, this case has to be considered unphysical.

The nature of the $\mathbf{q}$ structure in the dynamical structure factor can be readily followed as a function of the size of t_2. Associated with smaller t_2 are two general features: the incommensurability tends to decrease in magnitude while the depth of the minimum at the $(\pi/a,\pi/a)$ point tends to become deeper. To make the above remarks more quantitative, we present plots in Figs. 6(a)–6(c) of the magnitude of the incommensurability vector $\delta(x)$. Here, for simplicity, we consider the effects of the Lindhard function alone. We have found that in all models (appropriate to the La-Sr-Cu-O system), the RPA correction terms do not significantly change the position of the maxima in $\mathbf{q}$.

Figure 6(a) plots the incommensurability calculated (at $\omega\sim 10$ meV) using the present strong-U theory. As shown in the inset which replots data from Ref. 5, this figure is in reasonable agreement with experiment for $x<0.2$; above this hole concentration there are no experimental data. Because of Coulomb renormalization, the bands become progressively more narrow as $x\to 0$. In this way the spins become *localized* at the half-filled limit, as is expected of a Mott insulator. At $x=0$ the system can be described as a collection of Heisenberg spins (which interact antiferromagnetically).[42] Consequently the structure in the spin dynamics is associated with the $\mathbf{Q}_0$ point.[43] It is important to stress that in our theory the insulator is approached smoothly so that, even though our Fermi-liquid calculations are not appropriate for $x=0$, the finite x case extrapolates continuously to this limit. It should also be clear from the discussion in Sec. II B that this behavior of the continuously decreasing incommensurability is also related to the continuous decrease in the plasma frequency as the insulator is approached.

While the magnitude of the incommensurability is reasonably well described by $\delta(x)\sim 2x$ for $x<0.2$, we find that at sufficiently large x, the incommensurability begins to deviate from this linear dependence. This can be traced to the fact that the Coulomb renormalization of the tight-binding Hamiltonian parameters becomes progressively less important as the system becomes increasingly more metallic. Ultimately, the Fermi surface of the renormalized band structure is similar to that of the tight-binding case and the incommensurability loses its strong x dependence and begins to saturate, or even decrease slightly.

The rather good agreement between experiment and the present theory found in Fig. 6(a) may be contrasted with the results of Fig. 6(b). Here the incommensurabili-

ty in the one-band Hubbard case is plotted for a parametrization ($t_2/t_1=0.25$) in which the Fermi surface at $x=0.18$ is fitted to that of the three-band model. As noted above, the magnitudes of the incommensurability for moderate x are in reasonable agreement with experiment, but the x dependence is incorrect particularly at small x. A similar plot of the results for the limit $t_2=0$ is shown in Fig. 6(c). Here, the extrapolation to the $x=0$ limit is correct; however, the magnitudes of both $\delta(x)$ and slope $d\delta/dx$ are too small. These differences point to the importance of incorporating both reasonable Fermi-surface shapes, as well as strong Coulomb correlations (which are responsible for our x-dependent, Coulomb renormalized band structure).

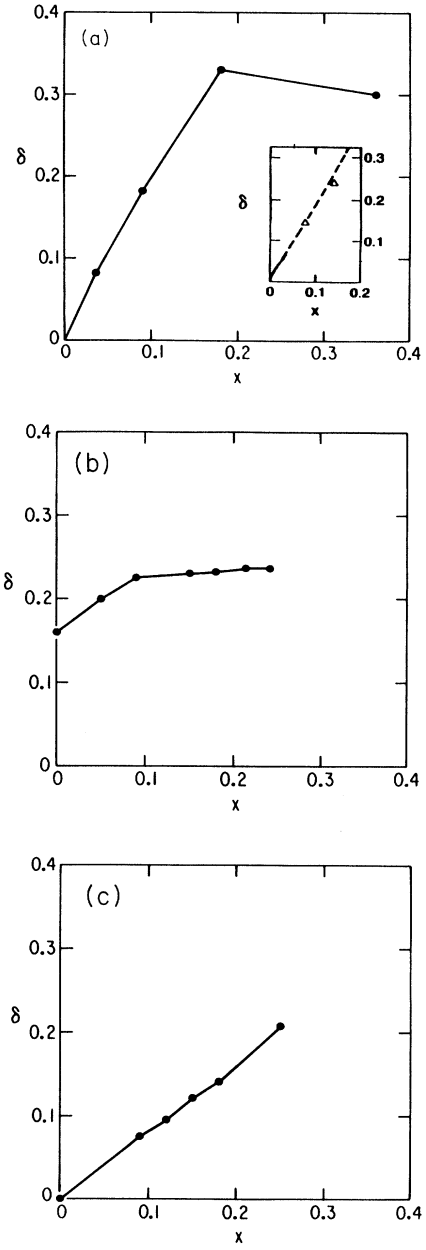

FIG. 6. Magnitude of incommensurability vector vs x in $La_{2-x}Sr_xCuO_4$ for Coulomb renormalized three-band case (a), for one-band $t_2/t_1=0.25$ case (b), and for one-band $t_2=0$ limit (c). The inset on (a) is from Ref. 5. The solid lines are guides to the eye.

We have briefly explored the frequency dependence of the incommensurability vector. This issue is complicated by the fact that the incommensurability arises from both nesting and singularity terms. The former are ω independent, whereas the latter are not. These singularity contributions approach $\mathbf{Q}_0$ as $\omega\rightarrow 0$. The net frequency dependence appears to be strongly dependent upon the amount of weight in $S(\mathbf{Q}_0,\omega)$ at moderate frequencies $\omega\sim 10$ meV. When this weight is low, we find the frequency dependence of the incommensurability to be essentially negligible, as was illustrated implicitly in Ref. 15, and as seems to be the case experimentally.[5]

IV. ENERGY SCALES IN MAGNETIC DATA: ω AND T DEPENDENCE

In this section we discuss the frequency and temperature dependence of the dynamical structure factor and the related (low) energy scales of the Fermi liquid. We plot our results as $\mathrm{Im}\chi(\mathbf{q},\omega)$ rather than $S(\mathbf{q},\omega)$, in order to separate out the boson factor. The latter contributes to frequency and temperature dependences which do not reflect the microscopic details of the system. For the Y-Ba-Cu-O family we focus on the $\mathbf{Q}_0=(\pi/a,\pi/a)$ point and for the La-Sr-Cu-O system we study the behavior around $\mathbf{Q}'$, where $\mathbf{Q}'=0.91(\mathbf{Q}_0)$ for $x=0.09$ and $0.85(\mathbf{Q}_0)$ for $x=0.18$. In this way, for both cuprates, the $\mathbf{q}$ values considered are at the maxima along the *zone diagonal direction* in the cross section.

In the $YBa_2Cu_3O_\delta$ systems, peaks have been observed[3,4] in $S(\mathbf{Q}_0,\omega)$ as a function of ω. In all cases the oxygen concentration δ was less than 7.[40] This peak structure is washed out as the temperature is increased so that at high T the behavior of $\mathrm{Im}\chi(\mathbf{Q}_0,\omega)$ appears to be linear in ω and T^{-1}. Neutron data[4] have revealed maxima in $S(\mathbf{Q}_0,\omega)$ at $\omega\sim 8$ meV for $\delta=6.5$ and $\omega\sim 25$ meV at $\delta=6.7$. In a general Fermi-liquid picture, for a $\mathbf{Q}_0$ comparable to the Fermi wave vector, $\mathrm{Im}\chi(\mathbf{Q}_0,\omega)$ increases montonically until slightly below the Fermi energy E_F, at which point it decreases rapidly to zero. Thus peak structure, when it is significantly below E_F, may be associated with fine structure in the density of states, such as Van Hove effects. Here the Van Hove energy E_{VH} corresponds to the separation between the Van Hove singularity and the Fermi energy. The frequency-dependent neutron data suggest that in this family of cuprates a characteristic electronic energy scale is roughly 25 meV for $O_{6.7}$ and decreases progressively as the insulator is approached. It should be stressed that because the peaks are associated with the low-T regime, it is important to ascertain that they are a consequence of the normal, rather than superconducting state. The clearest evidence for their role in the normal state is the observation[4] of 25-meV peaks at 75 K in a $T_c=59$ K sample. Furthermore, one may argue that the frequencies are sufficiently

high to be associated with the normal ("ungapped") regime.

Similar *temperature*-dependent maxima have been reported by one group[4] in $\mathrm{Im}\chi(\mathbf{Q}_0,\omega)$ data as a function of T for $YBa_2Cu_3O_{6.7}$ at sufficiently low $\omega \sim 8$ meV. Here the characteristic energy scale for this stoichiometry is of similar ($T \sim 15$ meV) magnitude. At higher ω, both $S(\mathbf{Q}_0,\omega)$ and $\mathrm{Im}\chi(\mathbf{Q}_0,\omega)$ decrease monotonically with T. It is not yet clear whether these phenomena have a counterpart in the La-Sr-Cu-O system, where the most detailed frequency and temperature analyses have focused on $\mathbf{q}$-integrated data in the low-x regime.[44] The results of the present section, which illustrate our predictions for the ω and T dependences of the cross section, should be viewed as important tests of the present Fermi-liquid model for La-Sr-Cu-O.

These predictions for La-Sr-Cu-O are shown in Figs. 7(a) and 7(b) for $x=0.09$ and 0.18, respectively. These figures plot the height of the zone diagonal (incommensurate) maximum $\mathbf{q}=\mathbf{Q}'$ in $\mathrm{Im}\chi$ as a function of ω for various temperatures. The strong peak structure seen at low $T=1$ meV is associated with the Van Hove energy scale, softened by spin-fluctuation effects. From the present studies, as well as from LDA calculations this energy, E_{VH}, is lowest at $x \sim 0.15$. We have found that $E_{\mathrm{VH}}=3$ meV for $x=0.09$ and 2 meV for $x=0.18$. These Van Hove energies tend to be lower than their counterparts in the Y-Ba-Cu-O system due to the different shape of the Fermi surface.

The temperature dependence in these curves also indicates a low-energy scale. Here the variations occur on the temperature scale of the "coherence" temperature,[17] T_{coh}, again slightly softened by spin fluctuations. The coherence energy may be viewed as an effective degeneracy temperature for the d electrons. As a result of strong Coulomb correlations, the bands are narrowed. Incipient localization produces a low T_{coh} which can be associated with some fraction ($\sim \frac{1}{4}$) of the separation between the Fermi energy and the nearest band edge. When $T > T_{\mathrm{coh}}$ these band-edge effects begin to be felt and the system no longer behaves as a fully degenerate (i.e., $T=0$) Fermi liquid.

It may be seen from Fig. 7 that at moderate temperatures, the sharp structure in $\mathrm{Im}\chi(\mathbf{Q}',\omega)$ versus ω has smoothed out and the behavior is reminiscent of the "marginal" ansatz.[45] It should be stressed that this similarity with the marginal ansatz should be associated only with ω or T larger than the Van Hove energy scale. When both ω and T are sufficiently small the marginal phenomenology does not apply. Similar conclusions have been reached by Virosztek and Ruvalds and coworkers.[13,46] In this context we have explored the nature of ω/T scaling[44] in the neutron cross section for the La-Sr-Cu-O family. At $x=0.18$ we have found an im-

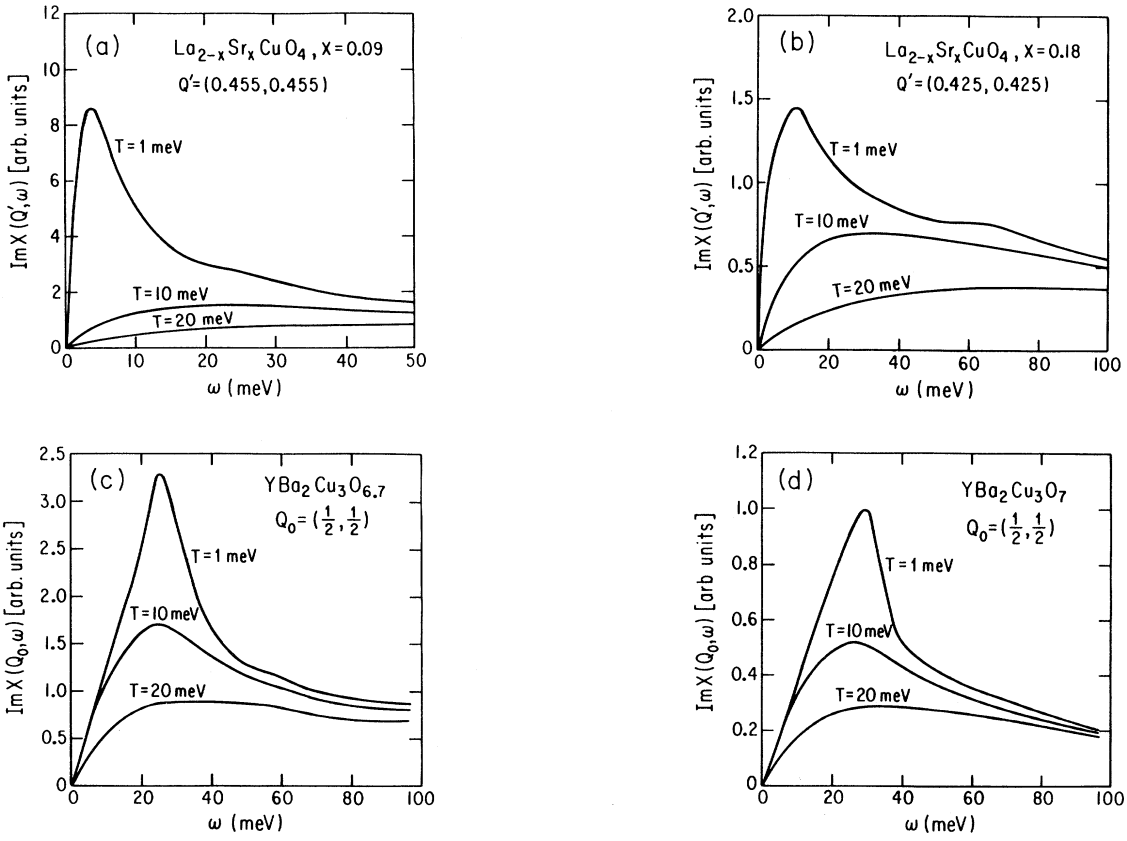

FIG. 7. Frequency dependence of $\mathrm{Im}\chi(\mathbf{q},\omega)$ at values of $\mathbf{q}$ corresponding to the position of its maximum value along the zone diagonal direction. The units of $\mathbf{q}$ are in terms of $(2\pi/a)$, (r.l.u.), and (a)–(d) represent the two cuprates at the indicated concentrations.

pressive scaling (i.e., with a "normalization" factor which is only weakly ω dependent[44]) of $S(\mathbf{Q}',\omega)$ for intermediate ($T > 5-8$ meV) and higher temperatures. Similar studies can be made for the Y-Ba-Cu-O system where the Van Hove energies are considerably higher. Here we predict that scaling will be less apparent than in the La-Sr-Cu-O family. Similar scaling effects have been reported experimentally[44] for this latter compound, although a complete survey of arbitrary wave vectors has not been undertaken. Results for this predicted scaling behavior are presented by Zha, Si, and Levin.[16]

Analogous plots of the frequency dependence of $\mathrm{Im}\chi(\mathbf{Q}_0,\omega)$ for the Y-Ba-Cu-O system are presented in Figs. 7(c) and 7(d) at the two oxygen stoichiometries. For sufficiently small temperatures, the Van Hove energy [softened by $J_H(\mathbf{q})$] leads to this peak structure. Here the maximum occurs at $\omega \sim 25$ meV for both cuprates and the Van Hove energy $E_{\mathrm{VH}} \sim 28$ meV for $O_{6.7}$ and $E_{\mathrm{VH}} \sim 25$ meV for O_7 are of the same scale. It is important to stress that for the $O_{6.7}$ system, the experimentally observed position[3,4] of the frequency maximum is consistent with these calculations. For higher oxygen concentrations the sharp maximum in $\mathrm{Im}\chi$ versus ω may not be visible since the normal-state temperatures are relatively high. In this context we note that the highest T plot in Fig. 7(d) is consistent with the observations of Bourges *et al.*[3] on the fully oxygenated system. It is worthwhile reiterating here the point that strong Coulomb correlations and associated narrow band effects necessarily lead to the low Van Hove energies,[18] shown in Fig. 7.

We end this series of figures by noting that the low-frequency behavior shown in Fig. 7 does not exhibit the "spin gap" effect reported in recent experiments[4,24] on Y-Ba-Cu-O. It is not yet clear whether this low-frequency decrease in the spectral weight is a consequence of the superconductivity or is a normal-state effect. As will be shown below, for low ω, in temperature-dependent plots as well as in plots of the Cu $1/T_1$ versus T, we do find a very slight indication of a so-called normal-state "spin gap" which we associate with the Van Hove effect. Further data is required to determine the origin of the experimental spin gap and its correlation with superconductivity in both Y-Ba-Cu-O and La-Sr-Cu-O systems.

Figures 8(a)–8(d) illustrate the temperature dependence of the neutron cross section at the $\mathbf{q}$ point where the intensity is maximum along the zone diagonal. Here, again, we focus on $\mathrm{Im}\chi$. We have found a maximum at the lowest frequencies which occurs as a function of temperature at roughly 0.6 of the Van Hove energy for both cuprates. This maximum is further softened by spin-fluctuation effects. For $La_{2-x}Sr_xCuO_4$ at both values of $x = 0.09$ and 0.18, the maximum is not visible on the

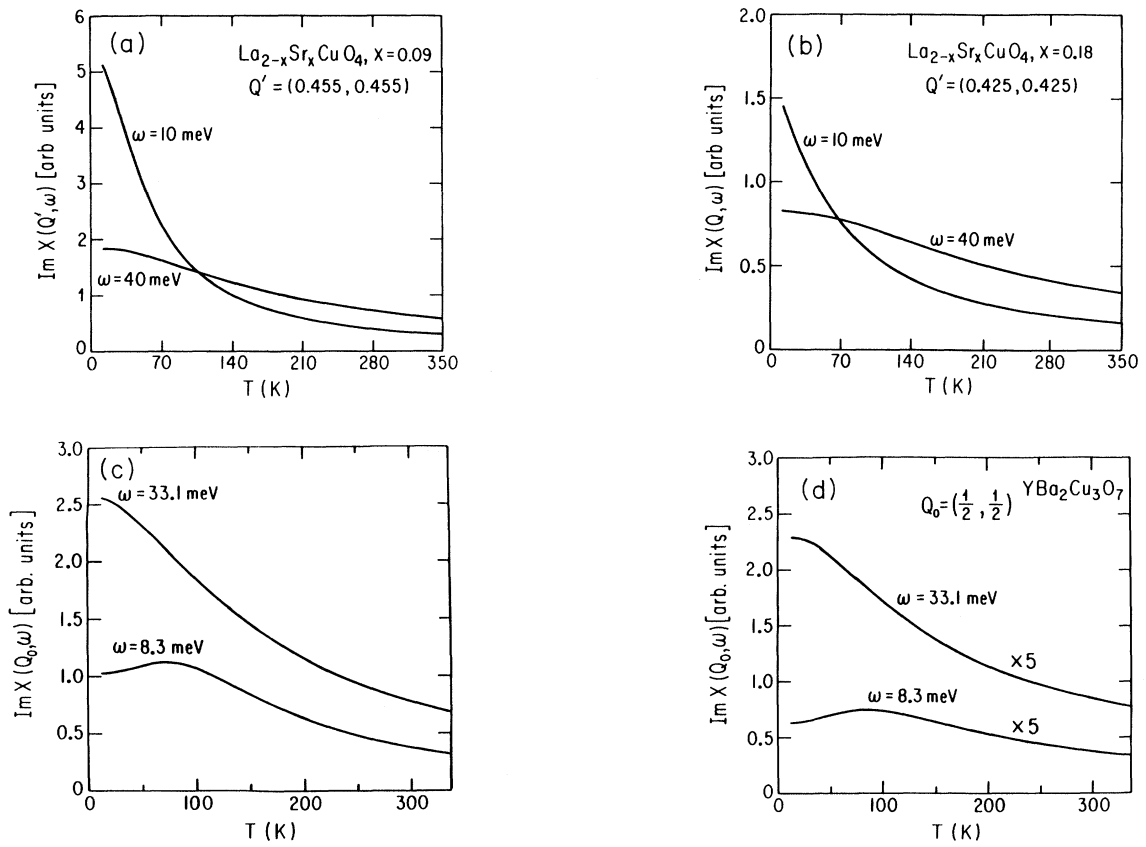

FIG. 8. Temperature dependence of $\mathrm{Im}\chi(\mathbf{q},\omega)$ at values of $\mathbf{q}$ corresponding to the position of its maximum value along the zone diagonal direction. Here two frequencies are shown and (a)–(d) represent the two cuprates at the indicated concentrations.

scale of Figs. 8(a) and 8(b), due to the relatively small Van Hove energy in these systems. Hence $\mathrm{Im}\chi(\mathbf{Q}',\omega)$ appears to decrease monotonically as a function of T. By contrast, Figs. 8(c) and 8(d), which are appropriate to the Y-Ba-Cu-O system, exhibit a low-temperature ($T\sim 8$ meV) peak at the lowest frequencies studied. This temperature is of the same order of magnitude, although somewhat lower than that observed in Ref. 4 for this oxygen stoichiometry. In addition, the higher-frequency ($\omega\sim 33$ meV) monotonic behavior appears to be consistent with the data in both Refs. 3 and 4.

V. NMR CALCULATIONS

The NMR relaxation rate is given by

$$(1/T_1)_r^{\alpha}=(T/2N_{\mathrm{site}})\sum_{\beta}{}' \sum_{r'r''}\sum_{\mathbf{q}} A_{rr'}^{\beta}(\mathbf{q})A_{rr''}^{\beta}(\mathbf{q}) \times \mathrm{Im}\chi_{r'r''}(\mathbf{q},\omega_0)/\omega_0 , \quad (7)$$

where ω_0 is the nuclear magnetic resonance frequency which can be taken to be zero. Here α and β label principal axes. The prime on the summation in Eq. (7) is over principal axes perpendicular to the field orientation α. The calculations of the present paper are based on the "standard models" for the hyperfine coupling constants[15] A_{dd}, A_{pp}, and A_{pd}.

$$A_{dd}^{ab}(\mathbf{q})=A_{dd}^{c}((A_{dd}^{ab}/A_{dd}^{c}) +2(B/A_{dd}^{c})[\cos(q_x a)+\cos(q_y a)]) , \quad (8a)$$

$$A_{dd}^{c}(\mathbf{q})=A_{dd}^{c}(1+2(B/A_{dd}^{c})[\cos(q_x a)+\cos(q_y a)]) , \quad (8b)$$

$$A_{p_x d}(\mathbf{q})=2A_{pd}\cos(q_x a/2) , \quad (8c)$$

$$A_{p_y d}(\mathbf{q})=2A_{pd}\cos(q_y a/2) . \quad (8d)$$

Of central concern in analyzing NMR data,[1,47–49] are the temperature dependences found for the Cu and O sites. In $YBa_2Cu_3O_7$ a Korringa ($1/T_1\propto T$) dependence occurs at both sites below $T\sim 120$ K. Above this T the oxygen NMR remains linear and the Cu relaxation begins to vary more slowly. The behavior away from optimal T_c as well as the NMR characteristics in the La-Sr-Cu-O family are more complicated. In general, at the lowest T of the normal state, the Cu NMR seems compatible with a linear temperature dependence, as in a canonical Fermi-liquid state. This behavior quickly gives way to a tendency towards saturation as T increases above T_c. Oxygen data[48] are consistent with Korringa behavior ($1/T_1\propto T$) in cuprates, near optimal stoichiometry over the entire normal-state regime. However, away from optimal stoichiometry (and in La-Sr-Cu-O) there appear to be deviations from this law, so that an approximation such as $1/T_1\propto\chi(T)T$ might be more appropriate. The deviations from a strict Korringa dependence thus reflect the T dependence of the static uniform susceptibility.

Here we focus primarily on the Cu relaxation, which is expected to be more directly related to neutron data. As we will show below, the experimentally observed relaxation at the O site is less easily understood in the context of the standard transfer hyperfine model which is subject to the constraints imposed by neutron data.[50] We argue that the narrow Korringa "window" at the Cu site suggests a breakdown of canonical Fermi-liquid behavior above a low characteristic temperature (energy). Further NMR support for a low-temperature Fermi liquid comes from overdoped cuprates,[51] where we have access to higher temperatures in the normal state. These materials, with reduced T_c, show a more extended Korringa regime which, as the superconductivity is suppressed, extends to lower and lower temperatures. In the remainder of this section we discuss the origin of the low- ("crossover") energy scale in the context of NMR data. We define the NMR energy scale operationally as the temperature above which Cu NMR exhibits deviations from the canonical Fermi-liquid Korringa dependence. For $La_{2-x}Sr_xCuO_4$ this deviation occurs[49] between 50 and 100 K for a range of x values around 0.15. (Indeed, this observation forms the basis for our phenomenological choice of J_0/J_c.) For $YBa_2Cu_3O_\delta$ we estimate that the deviation temperature is roughly[47] 150 K for $\delta=6.5$; results in the literature[48] suggest that this temperature corresponds to ~ 120 K for $\delta=7$. Although there is still considerable uncertainty in these numbers, it is clear that the characteristic NMR energy scales are of the order of ~ 10 meV or somewhat less.

Results for the Cu and O NMR are derived within the standard hyperfine coupling model, using the same $S(\mathbf{q},\omega)$ which was shown to be reasonably consistent with neutron measurements in both Y-Ba-Cu-O and La-Sr-Cu-O. Here we do not address Knight shift data. Spin susceptibility calculations for slightly different parametrizations have been presented elsewhere[15] and for optimal stoichiometry generally lead to Pauli-like temperature dependences. However, at lower x we fail to find the experimentally observed decrease in spin susceptibility[23] with decreasing T. It may be speculated that this requires a theory which goes beyond the RPA treatment of the present calculation. It has, furthermore, been argued in the literature that this T dependence is related to the low-frequency "spin gap" effect observed in neutron data. As yet, we have not addressed either of these issues.

Our calculations of the Cu and O relaxation rates in La-Sr-Cu-O are presented in Figs. 9(a) and 9(b) respectively. The Cu $1/T_1$ indicates a deviation temperature of 60 K for $x=0.09$ and 70 K for $x=0.18$. Below these T, the behavior is Korringa-like. These temperatures, which are in rough agreement with those measured experimentally, reflect the coherence energy scale T_{coh}. We have found[15] that the deviation occurs at temperature slightly lower than T_{coh}, at which point band-edge effects begin to be felt and the Cu NMR begins to saturate. The Van Hove energy, which is considerably lower than T_{coh} for this cuprate, plays a relatively minor role in the nuclear relaxation. This follows because $1/T_1$ involves contributions from all $\mathbf{q}$, so that this singularity is effectively integrated out. At the Van Hove temperature we find a rather weak residual feature which occurs in the Korringa regime. However, for La-Sr-Cu-O near optimal

stoichiometry (where the Van Hove energies are extremely low) it is expected to be hidden by the superconductivity.

The oxygen nuclear relaxation is generally assumed to arise via "transfer hyperfine" coupling,[20,21,47] so that the Cu spin-susceptibility component also relaxes the O sites. In this standard picture, oxygen can exhibit Korringa behavior, even when Cu NMR begins to saturate as a consequence of form factor cancellation effects: the contribution from a sufficiently sharp (antiferromagnetic) peak in $\mathrm{Im}\chi(\mathbf{Q}_0,\omega\sim 0)$ will cancel out on the oxygen site under ideal circumstances. However, we have found that this cancellation is imperfect due to the small size of the magnetic correlation length as well as to incommensurability effects. Because our calculations of $\mathrm{Im}\chi(\mathbf{q},\omega)$ are consistent with neutron data in both cuprates, we believe that this failure of the form factor cancellation arguments is a general result which may reflect the incompatibility of neutron and (oxygen) NMR measurements when the latter are described by the standard model in the literature. Similar claims have been made in a recent paper.[50] If in more conclusive measurements $1/T_1$ at the O site shows no evidence of a "leakage" of the Cu T dependence, one may be led to wonder whether mechanisms other than the transfer hyperfine relaxation may need to be included for a full understanding of the oxygen NMR.

The behavior of the Cu and oxygen relaxation is shown for the Y-Ba-Cu-O family in Figs. 9(c) and 9(d). The results are rather similar to those of La-Sr-Cu-O, except that the linear regime persists to somewhat higher temperatures. As noted above, the 25–30 meV Van Hove energy scale (which plays an important role in neutron data at fixed $\mathbf{q}=\mathbf{Q}_0$) is relatively unimportant for the NMR relaxation. Thus, it may be argued that even though NMR and neutron data reveal energy scales of the order of tens of millielectronvolts, these energy scales derive from different details of the quasiparticle energy dispersion. Nevertheless, the fact that these energies are of comparable magnitude reinforces the picture that they both represent the generally low-energy scales of the Fermi-liquid band structure. Comparing the relative size of $1/T_1$ for different oxygen concentrations [Fig. 9(c)], shows that the $1/T_1$ at the Cu site is about three times larger in the reduced oxygen sample. This difference is in the right direction, but somewhat larger than that observed experimentally.[47]

As found in the La-Sr-Cu-O system, the transfer hyperfine relaxation does not yield ideal Korringa behavior on the O site, as would be expected for the O_7 system. This result is again consistent with imperfect form factor cancellations associated with the generally large width of the antiferromagnetic peaks. Finally, we note that the relative size of the two oxygen relaxation rates shown in Fig. 9(d) is inverted with respect to the data.[48] Thus we

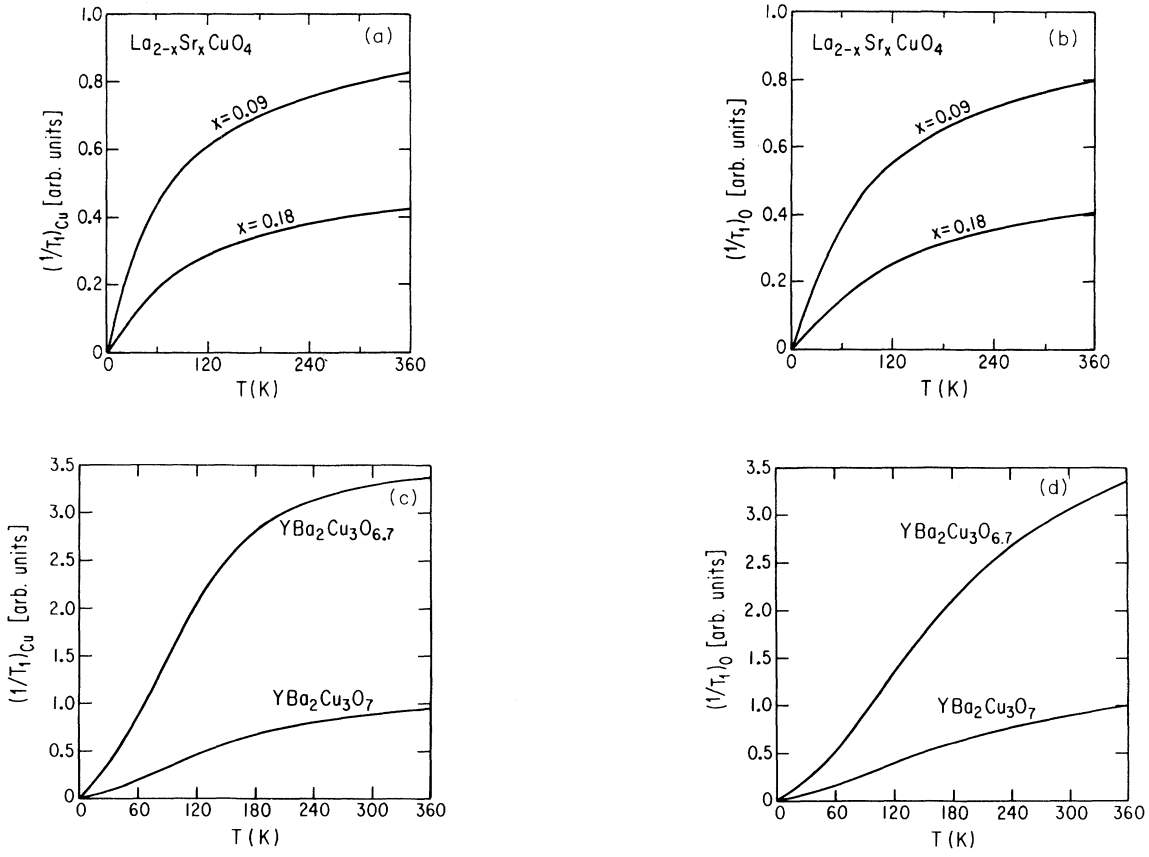

FIG. 9. Temperature dependence of NMR relaxation at the Cu (a),(c) and O (b),(d) sites in the two cuprates at indicated concentrations.

find that in the transfer hyperfine case the increase in the Cu component susceptibility with decreasing oxygen content is directly reflected in the size of the oxygen $1/T_1$. By contrast, experimentally, the O_7 system is found to have the larger $1/T_1$. These differences again point to our imperfect understanding of the oxygen relaxation mechanisms within the "standard" transfer hyperfine coupling NMR model, constrained by neutron data.

VI. LIFETIME EFFECTS

The low characteristic energy scales observed in these spin dynamical experiments have clear implications for a variety of other properties. Quite generally, these energies constrain the regime of validity of a canonical Fermi-liquid picture. Above the Van Hove, spin-fluctuation and/or coherence temperature, there will be important corrections to the $T=0$ Fermi-liquid picture. This forms an essential premise for all Fermi-liquid-based theories;[12,13,18,20,21] the variations from one theory to another all revolve around the microscopic source of the characteristic low-energy scales. Thus the low-energy scales are assumed to derive from near magnetism,[20,21] near localization,[12,17] near nesting,[13,46] and low Van Hove energies.[12,18] In reality some combination of all of these may be playing a role.

In this section, we discuss the crossover from quadratic to linear dependence (on temperature or frequency) in the quasiparticle lifetime. Here we focus on the role of the Van Hove effect on the quasiparticle lifetime which has been studied previously by others[12,13,52] as well as ourselves.[18] In our earlier work we argued that (1) a general consequence of strong Coulomb correlations is to lead to low Van Hove energies and (2) the Van Hove effect is relatively unique in that low-energy scales do *not* imply a low-temperature saturation in the lifetime. General electron-electron, unlike electron phonon scattering, yields such a saturation due to the temperature dependence of the electronic transport spectral function. Specific calculations of the lifetime were presented elsewhere[18] for the La-Sr-Cu-O family where, because of the band structure, the Van Hove energy is expected to be significantly smaller than in the Y-Ba-Cu-O system. Here we address this other cuprate family and show that with the parameters which seem appropriate to spin dynamical data, the lifetime also appears to be linear over the physically accessible regime. We also emphasize the energy scale at which the quadratic dependence may be seen for future analysis of low-frequency photoemission data. In this context we discuss some very recent interpretations of high-resolution Y-Ba-Cu-O photoemission experiments.[19]

Our expression for the quasiparticle lifetime, appropriate to a transport measurement is given by

$$\frac{1}{\tau_p}(T)=2g^2\int\frac{d\mathbf{p}_1}{\Omega}\frac{\chi''(\mathbf{p}-\mathbf{p}_1,\varepsilon_{\mathbf{p}_1})}{\sinh(\varepsilon_{\mathbf{p}_1}/T)}\ . \tag{9a}$$

Similarly for the photoemission line width we have

$$\frac{1}{\tau_p}(\varepsilon,T)=-2\,\mathrm{Im}\Sigma(\mathbf{p},\varepsilon)=g^2\int\frac{d\mathbf{p}_1}{\Omega}\chi''(\mathbf{p}-\mathbf{p}_1,\varepsilon-\varepsilon_{\mathbf{p}_1})\left[\tanh\frac{\varepsilon_{\mathbf{p}_1}}{2T}+\coth\frac{\varepsilon-\varepsilon_{\mathbf{p}_1}}{2T}\right], \tag{9b}$$

where Ω is the volume of the Brillouin zone. These expressions result from the lowest-order or "one loop" diagram. It should be stressed that these lowest-order diagrams are not fully self-consistent. Although, higher-order self-energy and vertex interactions should ultimately be included, Eqs. (9a) and (9b) are the standard starting point in the literature. Our results are summarized by Figs. 10 and 11, which plot the lifetime as a function of T and ω, for the O_7 system. Figure 10 indicates that the characteristic crossover from quadratic behavior is $\sim E_{\mathrm{VH}}/4$. Thus the Van Hove energy plays a similar crossover role as does the Debye energy for the phonon problem. Furthermore, the fraction of the characteristic energy scale ($\frac{1}{4}$) which governs the transport behavior is the same. Thus the resistivity becomes linear above ~ 7.5 meV, and remains linear until roughly $3-4T_{\mathrm{coh}}$ at which point band-edge effects become evident and corrections to a (degenerate) Fermi-liquid picture must be included.[53] We summarize this calculation by noting that even though the band structure of the Y-Ba-Cu-O family has a relatively large Van Hove energy, compared to the La-Sr-Cu-O system, this energy is still sufficiently small to enable the quadratic regime in the resistivity to be obscured by the superconductivity. Further support for the size of the Van Hove energy scale in $YBa_2Cu_3O_{6.7}$ comes from our analysis of neutron data, which is also consistent with $E_{\mathrm{VH}}\sim 20-30$ meV.

In Figure 11 we plot the frequency dependence of the lifetime for $YBa_2Cu_3O_7$. Here the dependence is quadratic until essentially the Van Hove energy is reached. Above this energy scale the behavior is linear and this linearity appears to persist to $\omega\sim 0.1$ eV. Recent very

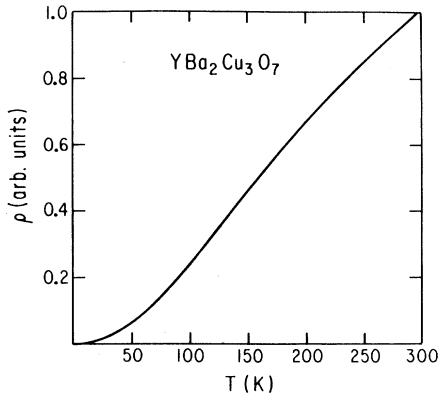

FIG. 10. Temperature dependence of the electronic component to the resistivity (quasiparticle lifetime) in $YBa_2Cu_3O_7$.

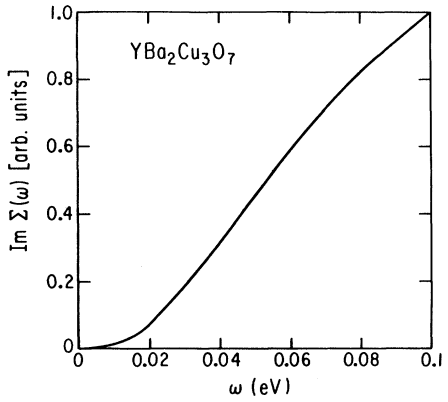

FIG. 11. Frequency dependence of the electronic component to the $T=0$ quasiparticle lifetime in $YBa_2Cu_3O_7$.

high resolution photoemission experiments[19] on this same system have been interpreted as providing evidence for a ω^2 to ω crossover at $\omega \sim 10-20$ meV. Our energy scale of 20–30 meV is reasonable although somewhat larger than this interpretation would suggest.

VII. CONCLUSIONS

In this paper we have emphasized the interconnection between fermiology and spin dynamics. Within a Fermi-liquid picture, these two are intimately related and measurements of the spin dynamics can be interpreted as a form of Fermi-surface spectroscopy. The main contribution of the present paper is to demonstrate that the different fermiology of the Y-Ba-Cu-O and La-Sr-Cu-O families is consistent with the differences observed in the ($\mathbf{q}$) dependence of the dynamical structure factor $S(\mathbf{q},\omega)$. Thus commensurate, temperature-independent peaks are observed as a function of $\mathbf{q}$ in the Y-Ba-Cu-O family, whereas temperature-dependent incommensurate peaks are found in the La-Sr-Cu-O system.

It is important to stress that, while our calculations are based on a particular and convenient theoretical "tool" (the $1/N$ expansion), the results are representative of a class of strong-U Fermi-liquid approaches. We would obtain similar results for $\chi^0(\mathbf{q},\omega)$ within an alternative Gutzwiller scheme[28] (at infinite U). We have also found that a phenomenological rescaling of the LDA-determined band parameters to the x-dependent plasma frequency, yields similar results. The phenomenological approach may be viewed as fitting the effective mass m^* via $\omega_p^2 \sim n/m^*$. The fact that the Drude fitted plasma data behave as $n/m^* \to 0$ as $x \to 0$ is closely related to the behavior of the renormalized hybridization $V_{pd}^* \to 0$, as $x \to 0$, which we have used here. It should also be noted that we have chosen only one parameter phenomenologically, namely, the amplitude of the antiferromagnetic coupling constant J_0, at one fixed (optimal) stoichiometry. The wave vector, hole concentration x, frequency, and temperature dependence of the net exchange $J_H(\mathbf{q})$ was calculated[14] using the same scheme as that which led to the Coulomb renormalized band structure. The latter gives rise to the Lindhard function $\chi^0(\mathbf{q},\omega)$. In this way all x dependences are deduced. Furthermore, this x dependence of the (various commensurate and incommensurate) $\mathbf{q}$ structure as well as the energy scales seem to be reasonably consistent with experiment.

These characteristic energy scales are quite apparent from spin dynamical measurements in the Y-Ba-Cu-O system. They appear as maxima, as functions of frequency and temperature in $\mathrm{Im}\chi(\mathbf{Q}_0,\omega)$. They also appear as the temperature below which Korringa behavior is seen on the Cu site in NMR experiments. Their characteristic size is of order ~ 10 meV. For the La-Sr-Cu-O family these maxima have not yet been observed in neutron data, although comparable characteristic temperatures appear in NMR experiments. Within a Fermi-liquid picture, these represent the energy scales of the Fermi liquid and are associated with Van Hove singularities E_{VH}, effective degeneracy temperatures T_{coh}, and spin-fluctuation frequencies. In our calculations we find that different measurements reflect slightly different combinations of these energy scales, for the most part all of reasonably comparable magnitude. The existence of these relatively low electronic energy scales can be seen to arise naturally within our formalism as a consequence of narrow band effects (deriving from strong Coulomb correlations) combined with *moderate* spin-fluctuation softening.

While we have emphasized that $\mathbf{q}$ structure in the spin dynamics reflects the fermiology, it is also clear that canonical Fermi-liquid (temperature and frequency) dependences are not seen in many experiments in the cuprates. The linear temperature dependence of the resistivity and the linear frequency dependence of the photoemission linewidth are inconsistent with the expected Fermi-liquid quadratic behavior. In this sense the cuprates cannot be described as canonical Fermi liquids. However, it is important to note that all observations of the normal state take place at temperatures comparable to the spin dynamical energy scales[1–5] of ~ 10 meV so that Fermi-liquid ground-state properties are not expected. In this paper we use our understanding of the spin dynamical energy scales (which are most clearly seen in neutron experiments on Y-Ba-Cu-O) to infer the temperature and frequency dependences of the electronic lifetime in this system. Our conclusion is that the quadratic Fermi-liquid temperature dependence in the resistivity is hidden by the superconductivity; for $T > T_c$ the temperature dependence is linear. Similarly the quadratic frequency dependence of the photoemission linewidth will not be seen, except in very high resolution experiments. Above a characteristic "crossover" frequency $\omega \sim 25$ meV, the expected frequency dependence is linear.

One aspect of the spin dynamics which is still not well resolved is the relation between the standard (transfer hyperfine coupling[20,21]) model for the O NMR and the neutron data. The present calculations of the O relaxation within this model do not yield sufficient form factor cancellations to explain the observed[1] Korringa behavior in $YBa_2Cu_3O_7$. Because these calculations yield reasonably good agreement with the antiferromagnetic peak widths as measured from the neutron experiments, this

seems to suggest either (1) that the finite-frequency neutron and "zero"-frequency NMR spin dynamics are different (2) that the standard NMR model needs to be improved, or finally (3) that either the NMR or neutron experiments are wrong. Our own experience with the ω dependence of the spin dynamics shows that the antiferromagnetic peak widths are essentially independent of ω in the Y-Ba-Cu-O family. In the La-Sr-Cu-O system the situation is somewhat more complicated (as discussed in Sec. III B) due to the nature of the incommensurate peak structure. However, here, too, we find that the form factor cancellations are inadequate to explain a complete decoupling between the T dependence of the Cu and O nuclear relaxations.

We end this paper with a summary of our general physical picture for the cuprates. Angular-resolved photoemission data provide, perhaps, the strongest evidence that these materials are "close to" a Fermi-liquid state. Here the measured band structure is found to be strikingly similar to that calculated within standard LDA schemes. On the other hand, transport and photoemission linewidth experiments indicate that the normal state is *not* a canonical (or ground-state) Fermi liquid. Rather than a characteristic quadratic Fermi-liquid dependence on temperature or frequency, the quasiparticle lifetime displays a linear dependence. We postulate that this linear dependence does not persist down to the $T \rightarrow 0$, $\omega \rightarrow 0$ limit (in the absence of superconductivity). In this sense these materials are not strictly "marginal",[45] although they may be indistinguishable from a marginal Fermi liquid at the *finite* temperatures and frequencies appropriate to normal state. The evidence for low-energy scales presented in this paper provides support for our scenario in which, at optimal stoichiometry, the crossover to the canonical Fermi liquid may be hidden by the relatively high temperatures of the normal state. The observation that in "overdoped" cuprates Fermi-liquid quadratic energy dependences are found[17] provides additional support. Finally, normal-state anomalies similar to those seen in the curates are found in the heavy fermion metals, above the canonical Fermi-liquid regime.[17] These materials can thus be viewed as a "road map" for the cuprates, since they are ground-state Fermi liquids which display (very) low-energy scales.

While there are now a number of different physical models[12,13,17,20,21] which introduce low-energy scales into a Fermi-liquid picture, it is not yet possible to distinguish unambiguously between them. The essence of the present picture is that strong Coulomb correlations lead to a "nearly localized" description of the Cu spins. In this way the system does not have to be tuned very close to a magnetic instability in order to explain the low- ($\sim$10 meV) energy scales of the spin dynamics. Narrow bandwidths already provide some reduction in the characteristic electronic energies. Indeed, it is difficult to believe that very "soft" magnetic fluctuations are solely responsible for these low-energy scales, particularly since in the Y-Ba-Cu-O family, the antiferromagnetic peaks at $\mathbf{Q}_0$ correspond to rather short (i.e., several lattice spacings) magnetic correlation lengths, even at reduced oxygen stoichiometries. Additional support for the present "nearly localized" scenario comes from the variation with decreasing hole concentration x of the plasma frequency and of the $\mathbf{q}$ structure in $S(\mathbf{q},\omega)$. In the present picture we find a smooth evolution in both the Y-Ba-Cu-O and La-Sr-Cu-O families towards *commensurate* and increasingly narrow antiferromagnetic peaks, as $x \rightarrow 0$. In this way, at half filling, the Fermi liquid gives way to a localized collection of Heisenberg spins at the Cu sites, which interact via the usual superexchange term.

Future experiments are clearly needed to test whether additional detailed aspects of the fermiology are indeed present in the spin dynamics. However, if the current differences between the $\mathbf{q}$ dependence of $S(\mathbf{q},\omega)$ in Y-Ba-Cu-O and La-Sr-Cu-O continue to hold up, these differences seem to provide confirmation of the importance of the fermiology to the spin dynamics of the cuprates.

Note added. We recently learned of related work by Littlewood, Zaanen, Aeppli, and Monien proposing a similar explanation for the $\mathbf{q}$ structure in La-Sr-Cu-O, which derives primarily from the fermiology. These authors use a marginal rather than Fermi-liquid-based approach, so that the strong T dependence of the neutron peaks derives from lifetime rather than low-energy scale effects. In another related work Ruvalds and co-workers have investigated a theory for explaining ω/T scaling within a Fermi-liquid-based approach. Presumably the nesting deviation temperature in their calculations plays a role similar to the Van Hove energy in the present theory. Fukuyama and co-workers have recently argued for the important effects of Fermi-surface shape on the spin dynamics using a very different (t-J) model for the cuprates. Their work confirms our explanation for the origin of the difference between the Y-Ba-Cu-O and La-Sr-Cu-O families. Finally, following our example, Pines and his co-workers have recently used the properly rotated Fermi-surface shape as well as a q-dependent spin exchange to describe NMR experiments in the Y-Ba-Cu-O family below T_c.

ACKNOWLEDGMENTS

We thank Ju Kim for his early collaborations. We acknowledge helpful conversations with J. M. Tranquada, J. J. Yu, and R. Benedek. We thank G. Aeppli and J. C. Campuzano for providing us with their respective data, prior to publication and for useful discussions. This work was supported by NSF-STC Grant No. STC-880954 and NSF-MRL Grant No. DMR-8819869.

*Present address: Serin Physics Laboratory, Rutgers University, Piscataway, NJ 08855-0849.

[1]For a review of NMR experiments in the copper oxides, see C. H. Pennington and C. P. Slichter, in *Physical Properties of High Temperature Superconductors,* edited by D. M. Ginsberg (World Scientific, Singapore, 1990).

[2]G. Shirane, R. J. Birgeneau, Y. Endoh, P. Gehring, M. A. Kastner, K. Kitazawa, H. Kojima, I. Tanaka, T. R. Thurston,

and K. Yamada, Phys. Rev. Lett. **63**, 330 (1989); For a review see R. J. Birgeneau and G. Shirane, in *Physical Properties of High Temperature Superconductors,* edited by D. M. Ginsberg (World Scientific, Singapore, 1989), Vol. I.

[3]J. M. Tranquada, in *Proceedings of the University of Miami Workshop on Electronic Structure and Mechanisms for High Temperature Superconductivity,* edited by J. Ashkenazi and G. Vazzoli (Plenum, New York, 1991). See also H. Chou, J. M. Tranquada, G. Shirane, T. E. Mason, W. J. L. Buyers, S. Shamoto, and M. Sato, Phys. Rev. B **43**, 5554 (1991); P. Bourges *et al., ibid.* **43**, 8690 (1991).

[4]J. Rossat-Mignod, L. P. Regnault, C. Vettier, P. Burlet, J. Y. Henry, and G. Lapertot, Physica B **169**, 58 (1991); see also J. Rossat-Mignod, Physica B **180-181**, 383 (1992).

[5]S.-W. Cheong, G. Aeppli, T. E. Mason, H. Mook, S. M. Hayden, P. C. Canfield, Z. Fisk, K. N. Clausen, and J. L. Martinez, Phys. Rev. Lett. **67**, 1791 (1991).

[6]J. C. Campuzano, G. Jennings, M. Faiz, L. Beaulaigue, B. W. Veal, J. Z. Liu, A. P. Paulikas, K. Vandervoort, H. Claus, R. S. List, A. J. Arko, and R. J. Bartlett, Phys. Rev. Lett. **64**, 2308 (1990).

[7]J. J. Yu, S. Massidda, A. J. Freeman, and D. D. Koelhing, Phys. Lett. A **122**, 203 (1987).

[8]R. Liu and B. Veal, J. Phys. Chem. Solids **52**, 1437 (1991); Rong Liu, B. W. Veal, A. P. Paulikas, J. W. Downey, P. J. Kostic, S. Fleshier, U. Welp, C. G. Olson, X. Wu, A. J. Arko, and J. J. Joyce, Phys. Rev. B **45**, 5614 (1992).

[9]O. K. Anderson *et al.*, Physica C **185-189**, 147 (1991).

[10]L. F. Mattheiss, Phys. Rev. Lett. **58**, 1028 (1987); J. Yu, A. J. Freeman, and J. H. Xu, *ibid.* **58**, 1035 (1987).

[11]W. E. Pickett, Rev. Mod. Phys. **61**, 433 (1989).

[12]D. M. Newns, P. C. Pattnaik, and C. C. Tsuei, Phys. Rev. B **43**, 3075 (1991).

[13]J. Ruvalds and A. Virosztek, Phys. Rev. B **42**, 4064 (1990).

[14]Q. Si, J. P. Lu, and K. Levin, Phys. Rev. B **45**, 4930 (1992); Physica C **162-164**, 1467 (1989). These calculations also investigated the role of varying V_{pd}, for both large and small t_{pp}. In the former case, the RKKY interaction is found to dominate only at relatively small V_{pd}. As this hybridization increases, we find the RKKY component is substantially reduced, while the superexchange contribution is much less affected. By contrast, in the limit of vanishing t_{pp} the RKKY interaction is suppressed by a factor of the hole concentration x; here the superexchange contribution dominates for most values of x.

[15]J. P. Lu, Qimiao Si, Ju H. Kim, and K. Levin, Phys. Rev. Lett. **65**, 2466 (1990); Physica C **179**, 191 (1991).

[16]For the renormalized band structure of La-Sr-Cu-O see J. H. Kim, K. Levin, and A. Auerbach, Phys. Rev. B **39**, 11 633 (1989). A discussion of the Coulomb renormalized band structure and related spin dynamical effects in Y-Ba-Cu-O can be found in Y. Zha, Q. Si, and K. Levin, Physica C **201**, 289 (1992). For studies of susceptibility scaling and bilayer effects, see Y. Zha, Q. Si, and K. Levin (unpublished).

[17]For a review see K. Levin, Ju H. Kim, J. P. Lu, and Q. Si, Physica C **175**, 449 (1991).

[18]Q. Si and K. Levin, Phys. Rev. B **44**, 4727 (1991).

[19]As pointed out by Hodges *et al.* [Phys. Rev. B **4**, 302 (1971)], strictly speaking, in two-dimensional systems the expected Fermi-liquid dependence is $T^2 \ln T$ or $\omega^2 \ln \omega$. However, the logarithmic corrections are not substantial and throughout this paper we will refer to the Fermi-liquid power laws as quadratic. In recent high-resolution photoemission experiments [J. C. Campuzano, G. Jennings, A. J. Arko, R. S. List, and R. Benedek, J. Phys. Chem. Solids **52**, 1411 (1991)], a quadratic frequency dependence has been claimed for $\omega < 20$ meV.

[20]A. J. Millis, H. Monien, and D. Pines, Phys. Rev. B **42**, 167 (1990). Here and in the following reference the oxygen relaxation is based on the transfer-hyperfine coupling model of F. Mila and T. M. Rice, Physica C **157**, 561 (1989).

[21]N. Bulut, D. Hone, D. J. Scalapino, and N. E. Bickers, Phys. Rev. Lett. **64**, 2723 (1990); Phys. Rev. B **41**, 1797 (1990).

[22]B. Shraiman and E. Siggia, Phys. Rev. Lett. **62**, 1564 (1989); C. L. Kane, P. A. Lee, T. K. Ng, B. Chakraborty, and N. Read, Phys. Rev. B **41**, 2653 (1990); P. Hedegard and M. B. Pedersen, *ibid.* **42**, 10 035 (1990).

[23]J. B. Torrance, A. Bezinge, A. Nazzal, T. Huang, S. Parkin, D. Keane, S. LaPlaca, P. Horn, and G. Held, Phys. Rev. B **40**, 8872 (1989); M. Takigawa *et al., ibid.* **43**, 247 (1991); W. Warren *et al.*, Phys. Rev. Lett. **62**, 1193 (1989).

[24]Rossat-Mignod *et al.* (see Ref. 4); P. M. Gehring, J. Tranquada, G. Shirane, J. Copley, R. Erwin, M. Sato, and S. Shamoto, Phys. Rev. B **44**, 2811 (1991).

[25]An application of the $1/N$ technique to the cuprates (including mean-field and higher-order corrections) can be found in G. Kotliar, P. A. Lee, and N. Read, Physica C **153-155**, 11 633 (1988).

[26]Because of their complexity, we did not solve the mean-field equations at finite T. Although qualitatively correct at somewhat higher T, the Fermi-liquid approach begins to break down for $T > T_{\rm coh}$.

[27]P. Coleman, Phys. Rev. B **35**, 5072 (1987).

[28]T. M. Rice and K. Ueda, Phys. Rev. Lett. **55**, 995 (1985); see also B. Brandow, Phys. Rev. B **37**, 250 (1988).

[29]M. Suzuki, in *Strong Correlation and Superconductivity,* edited by H. Fukuyama, S. Maekawa, and A. P. Malozemoff (Springer-Verlag, New York, 1989).

[30]J. Orenstein, G. A. Thomas, A. J. Millis, S. L. Cooper, D. H. Rapkine, T. Timusk, L. F. Schneemeyer, and J. V. Wasczak, Phys. Rev. B **42**, 6342 (1990).

[31]These O-O overlap terms can be seen to be essential in order to explain the positive Hall coefficient which reflects the curvature of the Fermi surface. See Ref. 16.

[32]A similar demonstration that next-nearest-neighbor hopping processes can give rise to the rotated Fermi surface of Y-Ba-Cu-O was presented in Ref. 7 in the context of a one-band Hubbard model.

[33]A. K. McMahan, R. M. Martin, and S. Satpathy, Phys. Rev. B **38**, 6650 (1988); M. Hybertsen, M. Schluter, and N. Christensen, *ibid.* **39**, 9028 (1989); E. Stechel, in *High Temperature Superconductivity: Proceedings of the Los Alamos Symposium, 1989,* edited by K. S. Bedell, D. Coffey, D. E. Meltzer, D. Pines, and J. R. Schrieffer (Addison-Wesley, Redwood City, CA, 1990).

[34]Additional estimates of the planar hole concentration can be provided by the LDA-calculated volume of the Fermi surface. We note, however, that this comparison is made difficult by the fact that ours is a strictly two-dimensional model, whereas the calculations of Ref. 7 contain some dispersion in the third direction.

[35]A. Auerbach, J. H. Kim, K. Levin, and M. R. Norman, Phys. Rev. Lett. **60**, 623 (1988).

[36]H. J. Schultz, Phys. Rev. Lett. **64**, 1445 (1990) has found similar incommensurate peaks along the zone edge (rather than zone diagonal) in a one-band nearest-neighbor tight-binding model. See also A. Moreo *et al.*, Phys. Rev. B **41**, 2313 (1990).

[37]Note that we did not attempt to match the volume of the model two-layer Fermi surface to our one CuO_2 layer model. The former is a reasonably good representation of the LDA-calculated Fermi surfaces of Ref. 7, which has a surprisingly low hole concentration.

[38]J. M. Tranquada, G. Shirane, B. Keimer, S. Shamoto, and M. Sato, Phys. Rev. B **40**, 4503 (1989).

[39]Note that this lifetime broadening (which enters into the band-structure singularity contribution in La-Sr-Cu-O) does not have a counterpart in the commensurate peak of Y-Ba-Cu-O, since the latter derives from the $\mathbf{q}$ dependence of $J(\mathbf{q})$, which is T independent.

[40]Since this paper was submitted Rossat-Mignod has claimed to see the O_7 peak with a width $\Delta q = 0.3$, and a peak in the ω dependence at $\omega \sim 40$ meV. See J. Rossat Mignod *et al.*, Physica C **185-188**, 86 (1991).

[41]The presence of a nonzero t_2 which is indicated by neutron experiments (via the size of the incommensurability at finite x) as well as by Hall data (via the sign of the Hall coefficient) makes it difficult to treat the magnetism at $x = 0$ as deriving from a spin-density wave (SDW); the SDW picture requires very strong nesting which may not be present.

[42]As demonstrated in Ref. 14, the present form for $J_H(q)$ extrapolates smoothly to the usual antiferromagnetic superexchange interaction of the insulator.

[43]Mathematically, this point can be understood as follows: at the half-filled limit ($x = 0$), our self-consistent mean-field solution yields $e_0 = 0$, as expected for a Brinkman-Rice or Mott insulator. In this limit the Cu and O states are effectively decoupled and one would expect the characteristic wave vector associated with the Cu sites to reflect the underlying copper lattice with nesting vector $\mathbf{Q}_0 = (\pi/a, \pi/a)$.

[44]Scaling effects in the La-Sr-Cu-O system at low x were reported by S. M. Hayden, G. Aeppli, H. Mook, D. Rytz, M. F. Hundley, and Z. Fisk, Phys. Rev. Lett. **66**, 821 (1991); B. Keimer, R. J. Birgeneau, A. Cassanho, Y. Endoh, R. W. Erwin, M. A. Kastner, and G. Shirane, *ibid.* **67**, 1930 (1991). Higher x studies (see, e.g., Ref. 2) have not yet addressed this scaling. Sternlieb *et al.*, Phys. Rev. B **47**, 5320 (1993) have recently demonstrated scaling in the Y-Ba-Cu-O system.

[45]C. M. Varma *et al.*, Phys. Rev. Lett. **63**, 1996 (1989).

[46]J. Ruvalds, C. Rieck, J. Zhang, and A. Virosztek, Science **256**, 1667 (1992).

[47]See, for example, H. Alloul, T. Ohno, and P. Mendels, Phys. Rev. Lett. **63**, 1700 (1989); S. E. Barrett, D. J. Durand, C. H. Pennington, C. P. Slichter, T. A. Friedmann, J. P. Rice, and D. M. Ginsberg, Phys. Rev. B **41**, 6283 (1990); M. Horvatic, P. Segarnsan, C. Berthier, Y. Berthier, P. Butaud, J. Y. Henry, M. Couach, and J. P. Chaminade, *ibid.* **39**, 7332 (1989); T. Imai, H. Yasuoka, T. Shimizu, Y. Ueda, K. Yoshimura, and K. Kosuge, Physica C **162-164**, 169 (1989); W. W. Warren, R. E. Walstedt, G. F. Brennert, R. J. Cava, R. Tycko, R. F. Bell, and G. Dabbagh, Phys. Rev. Lett. **62**, 1193 (1989).

[48]P. C. Hammel, M. Takigawa, R. H. Heffner, Z. Fisk, and K. C. Ott, Phys. Rev. Lett. **63**, 1992 (1989); M. Takigawa *et al.*, Phys. Rev. B **43**, 247 (1991).

[49]Y. Kitaoka, S. Ohsugi, K. Ishida, and K. Asayama, Physica C **170**, 189 (1990); T. Imai, K. Yoshimura, T. Uemura, H. Yasuoka, and K. Kosuge, J. Phys. Soc. Jpn. **59**, 3846 (1990).

[50]This observation has also been made by A. J. Millis and H. Monien, Phys. Rev. B **45**, 3059 (1992).

[51]Y. Kitaoka, K. Ishida, S. Ohsugi, K. Fujiwara, G.-q. Zheng, and K. Asayama, Appl. Magn. Reson. **3**, 549 (1992); Y. Kitaoka, K. Fujiwara, K. Ishida, K. Asayama, Y. Shimakawa, T. Manako, and Y. Kubo, Physica C **179**, 107 (1991).

[52]P. A. Lee and N. Read, Phys. Rev. Lett. **58**, 2691 (1987).

[53]Indeed, one could argue quite generally that the present picture (which includes temperature only through a thermal smearing effect) should not be applied when T (or ω) exceeds temperatures of the order of $3-4T_{coh}$.